AGU PUBLICATIONS

Paleoceanography

RESEARCH ARTICLE
10.1002/2014PA002652

Key Points:
- STF discontinuous south of NZ during glacial
- STF shifts south during the deglacial and early Holocene
- Position and strength of STF related to the Southern Hemisphere westerly winds

Correspondence to:
H. Bostock,
Helen.Bostock@niwa.co.nz

Citation:
Bostock, H. C., B. W. Hayward, H. L. Neil, A. T. Sabaa, and G. H. Scott (2015), Changes in the position of the Subtropical Front south of New Zealand since the last glacial period, *Paleoceanography*, *30*, 824–844, doi:10.1002/2014PA002652.

Received 3 APR 2014
Accepted 27 MAY 2015
Accepted article online 29 MAY 2015
Published online 14 JULY 2015

Changes in the position of the Subtropical Front south of New Zealand since the last glacial period

Helen C. Bostock[1], Bruce W. Hayward[2], Helen L. Neil[1], Ashwaq T. Sabaa[2], and George H. Scott[3]

[1]National Institute of Water and Atmospheric Research, Greta Point, New Zealand, [2]Geomarine Research, St Johns, New Zealand, [3]GNS Science, Lower Hutt, New Zealand

Abstract This study fills an important gap in our understanding of past changes in the Southern Subtropical Front (S-STF) in the southwest Pacific Ocean. Paleo-sea surface temperatures (SST) were estimated from planktic foraminiferal census counts from cores straddling the modern S-STF in the Solander Trough, south of New Zealand. The estimated SST were compared for 6 time slices; glacial period (25–21 ka), Last Glacial Maximum (LGM; 21–18 ka), early deglaciation (18–16 ka), late deglacial/early Holocene period (14–8 ka), mid-Holocene period (8–4 ka), and late Holocene period (4–0 ka). The position of the S-STF was determined by two methods: (1) the location of the 10°C isotherm and (2) the location of the highest SST gradients. These new results suggest that the S-STF was not continuous between east and west of New Zealand during the glacial period. Steep SST gradients indicate that a strong S-STF rapidly shifted south during the LGM and early deglaciation. During the late deglacial and Holocene periods the position of the S-STF differs between the two methods with reduced SST gradients, suggesting a more diffuse S-STF in the Solander Trough at this time. The glacial SST data suggest that the S-STF shifted north to the west of New Zealand, while to the east there was a stronger SST gradient across the front. This was possibly the result of an increased wind stress curl, which could have been caused by stronger, or more northerly Southern Hemisphere westerly winds (SHWW), or a merging of the SHWW split jet in this region.

1. Introduction

The Subtropical Front (STF) is traditionally considered to be the northern extent of the Southern Ocean forming a major frontal zone and water mass boundary that separates the warm, salty surface waters of the subtropical gyre from the cold, fresh subantarctic surface waters associated with the Antarctic Circumpolar Current (ACC) [*Orsi et al.*, 1995; *Belkin and Gordon*, 1996]. The position and intensity of the STF, and the processes that occur at the front, have a significant influence on the heat, salt, and nutrient exchange between the Southern Ocean and the subtropical gyres. The STF is also a region of high biological productivity with the mixing of micronutrient-rich subtropical waters (STW) with macronutrient-rich subantarctic waters (SAW) [*Boyd et al.*, 1999] and is subsequently also an important sink for atmospheric CO_2 [*Currie et al.*, 2011].

In the last decade with increasing data from conductivity-temperature-depths (CTDs), satellites, Argo floats, and climate models our traditional understanding of the position, continuity, and dynamics of the STF has been challenged [*Sokolov and Rintoul*, 2009; *Graham and De Boer*, 2013; *De Boer et al.*, 2013]. This has implications for using paleo-temperature proxy data to interpret changes in the location of the STF as a water mass boundary and inferences in the paleo-strength and latitude of the Southern Hemisphere westerly winds (SHWW) [*Kohfeld et al.*, 2013].

The goal of this paper is to use closely spaced deep-sea marine sediment cores from the Solander Trough, south of New Zealand (Figure 1), to reconstruct past changes in the Southern STF (S-STF). This transect of cores fills a critical gap in our spatial knowledge of the S-STF in the southwest Pacific Ocean. We use two methods for reconstructing the fronts: (1) identifying a specific isotherm associated with the modern S-STF (10°C) and (2) identifying the strongest SST gradients. We examine changes during the following time slices: glacial period (25–21 ka), Last Glacial Maximum (LGM; 21–18 ka), early deglacial period (18–16 ka), late deglacial/early Holocene period (14–8 ka), mid-Holocene period (8–4 ka), and late Holocene period (4–0 ka). The data from this study are compared to other regional reconstructions of the S-STF in the southwest

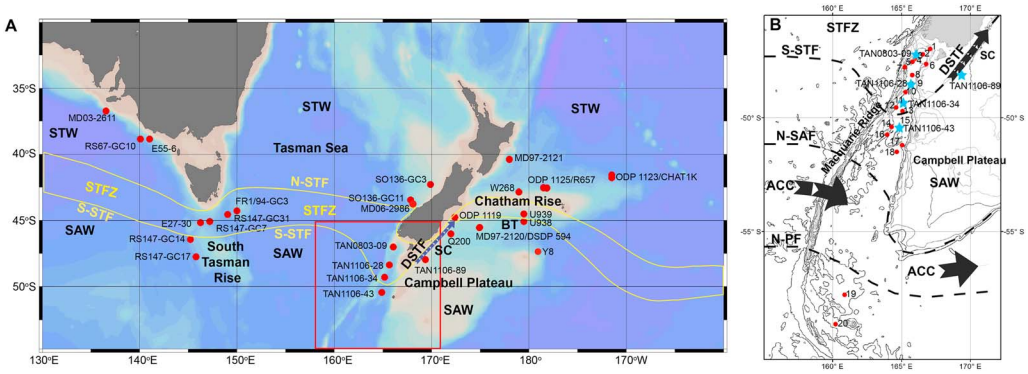

Figure 1. (a) Map of the southwest Pacific Ocean with the location of the Subtropical Frontal Zone–STFZ, Southern Subtropical Front–S-STF, Northern Subtropical Front–N-STF, and Dynamic Subtropical Front–DSTF and the cores discussed in the text (Table 1). Map created in Ocean Data View [*Schlitzer*, 2009]. (b) Detailed map of the location of the S-STF south of New Zealand [*Smith et al.*, 2013] and location of the R/V *Tangaroa* cores (blue stars) and core tops/surface samples (red circles) used in this study (Table 2). The N-SAF (northern Subantarctic Front) and the N-PF (northern Polar Front) adapted from *Sokolov et al.* [2006] are also shown in Figure 1b.

Pacific Ocean and combined with the new understanding of the modern processes to better infer the implications of these frontal shifts in terms of surface circulation and Southern Hemisphere westerly wind (SHWW) dynamics.

1.1. Subtropical Front

Traditionally, the STF has been depicted as an almost continuous (except for the South American sector [*Orsi et al.*, 1995] single front around the Southern Hemisphere. The STF was defined by a strong temperature (4°C) and salinity gradient (~0.7) over 1° latitude at approximately 40°S [*Deacon*, 1982; *Belkin and Gordon*, 1996]. However, detailed hydrographic studies around the Southern Ocean discovered that the convergence of the STW and SAW occurs over a wide Subtropical Frontal Zone (STFZ), up to 500 km wide (Figure 1a) and is defined by two sharp fronts—the North STF (N-STF) and the S STF [*Belkin and Gordon*, 1996; *Sutton*, 2001; *Kostianoy et al.*, 2004; *Burls and Reason*, 2006; *Hamilton*, 2006]. Typically, the N-STF is a shallower feature which defines the northern extent of the modified SAW, while the deeper S-STF is the main STF that was previously recognized and is the poleward extent of the STW [*Hamilton*, 2006].

Over the last decade sea surface temperature (SST) and sea surface height (SSH) data from satellites have been used to trace the fronts around the Southern Ocean [e.g., *Sokolov and Rintoul*, 2002]. The results have challenged the traditionally held paradigm of a continuous S-STF with associated currents. Recently, the S-STF has been redefined as two fronts controlled by different mechanisms: (1) a dynamical subtropical front (DSTF), which is associated with the strong flows (from SSH) of the western boundary currents and is stationary throughout the year, (2) and the southern edge of a broad STFZ in the center or eastern side of the Southern Hemisphere basins, which has no flow and shifts seasonally [*Graham and De Boer*, 2013]. In the summer months these two fronts appear to join up, but in the winter they are separated by several degrees of latitude. Thus, the S-STF, as defined by steep SST gradients, is not a continuous front [*Graham and De Boer*, 2013]. As a result of this new understanding of the S-STF, the traditional relationship between the front and wind stress curl has also been challenged, especially as it varies considerably in different regions [*De Boer et al.*, 2013].

1.2. Regional Setting

South of New Zealand there are two major bathymetric features that influence the oceanography of the region—Macquarie Ridge and Campbell Plateau. The Macquarie Ridge has an average depth of 1000 m, but varies from 4000 m water depth at gaps in the ridge, to seamounts that come to within 100 m, or in the case of Macquarie Island, currently sit above present sea level [*Conway et al.*, 2012] (Figure 1b). Further to the east sits the Campbell Plateau, which is a submerged continental platform. The plateau has an average depth of 600–1000 m, with a number of shallower rises and islands [*Neil et al.*, 2004]. Both the Macquarie Ridge and the Campbell Plateau form significant topographic barriers to water flowing around the south of New Zealand [*Neil et al.*, 2004; *Sokolov et al.*, 2006; *Smith et al.*, 2013].

Between the Macquarie Ridge and the Campbell Plateau sits the narrow (100–130 km), elongate Solander Trough, which begins at about 500 m water depth at 46.5°S and extends in a south-southwesterly orientation for 550 km down to depths of 4000 m at 51°S. Sediment, primarily produced by the erosion from New Zealand's Southern Alps, is transported from the South Island of New Zealand down the Solander Trough and has produced a thick sequence of terrigenous and hemipelagic sediments within the Solander Trough [*Schuur et al*., 1998].

1.3. Local Oceanography

Upstream of the Solander Trough, in the Tasman Sea, CTD, satellite and Argo data show that the S-STF is a diffuse feature, conforming to the definition of the STFZ, which is density compensated (no flow), [*Hamilton*, 2006; Smith and Vennell, in review]. Downstream of the Solander Trough the S-STF is a well-defined narrow front with a strong flow northeast along the edge of the continental shelf and conforms to the definition of the DSTF [*Graham and De Boer*, 2013]. Here it is locally known as the Southland Current and transports as much as 8.3 Sv, but predominantly transports SAW [*Heath*, 1985; *Shaw and Vennell*, 2001; *Sutton*, 2003; *Hopkins et al*., 2010] (Figures 1a and 1b).

Numerous researchers have previously attempted to define the location of the S-STF within the Solander Trough (reviewed by *Smith et al*. [2013]). Recently, a comparison of satellite SST data and hydrographic data collected during April–May 2011 identified the S-STF from the surface SST gradient (a sharp SST drop from 12–10°C) and a mixed layer salinity maximum south of New Zealand (Figure 1b) [*Smith et al*., 2013]. A well-defined S-STF sits just north of a shallow (~100 m) seamount on the Macquarie Ridge around 49.5°S, while in the deep Solander Trough (>3000 m at this latitude) the S-STF is less well defined, and two fronts were identified at 49°S and 50°S (150 km apart). The most southerly S-STF may be related to the presence of an eddy at the time of the voyage. In the Solander Trough the S-STF is predominantly density compensated [*Smith et al*., 2013] with little flow (~2 Sv [*Morris et al*., 2001]). However, this is the transition zone between the STFZ (upstream) and the DSTF (downstream). On the eastern side of the Solander Trough the S-STF is blocked by the Campbell Plateau and is topographically steered by the bathymetry through the ~800 m Snares Depression, where it once again becomes a well-defined narrow front (28 km), which is associated with the 500 m isobath and a strong flow (Figure 1b) [*Smith et al*., 2013], forming the start of the Southland Current.

Just 2.5° to the south of the S-STF along the Macquarie Ridge lies the Subantarctic Front (N-SAF; Figure 1b), the northern boundary of the ACC. The N-SAF has been identified from the SSH signature, flowing through a gap in the Macquarie Ridge at 52°S [*Sokolov et al*., 2006]. The northern-most Polar Front (N-PF) in this region is present at another gap in the ridge at ~56°S [*Sokolov et al*., 2006] (Figure 1b).

1.4. Previous Work

Significant changes in the estimated paleo-SST from numerous cores during the last glacial period have led many researchers to suggest that the position of S-STF shifted equatorward by 3–5° at numerous locations across the Southern Hemisphere oceans (reviewed in *Kohfeld et al*. [2013] who defined the LGM as 19–23 ka). These studies used a range of different floral, faunal, and geochemical proxies, and it should be noted that each proxy will produce subtly different SST estimates due to the organisms association with different seasons and habitats. Coccolithophores, that produce the alkenones, predominantly grow in stratified surface waters in summer, and thus, alkenone SST are more likely related to summer SST [*Sikes et al*., 2002; *Sikes et al*., 2005]. In contrast, the foraminiferal assemblages in this region represent the mean annual SST (which is similar to the spring SST), as the highest production and sediment fluxes is in spring [*King and Howard*, 2001; *Sikes et al*., 2002; *Northcote and Neil*, 2005].

A brief summary of the previous work is presented here and will be expanded on in the discussion (section 4.2). In the southwest Pacific Ocean the paleo-SST evidence suggests that south of Australia and in the Tasman Sea the S-STF was ~4° further north during the glacial period [*Howard and Prell*, 1992; *Passlow et al*., 1997; *Calvo et al*., 2007; *Sikes et al*., 2009; *Hayward et al*., 2012]. In contrast, the position of the STF east of New Zealand is considered to have remained locked to the Chatham Rise during the glacial-Holocene, probably due to topographic control imposed by the shallow bathymetry [*Weaver et al*., 1998; *Sikes et al*., 2002]. South of the Chatham Rise the SST during some glacial periods in the middle and late Pleistocene was so cool at ODP site 1119 (Figure 1a) that it was unlikely that any STW passed around the south of the South Island of

New Zealand. During the last glacial, however, SST estimates for ODP site 1119 were only 2°C cooler than present and it has been suggested that some STW leaked around the southern South Island and northward up the coast over this core site [*Wilson et al*., 2005; *Hayward et al*., 2008, 2012].

The missing piece of this glacial puzzle has been south of New Zealand. This research fills this gap and uses SST estimates based on foraminiferal assemblages from a transect of cores in the Solander Trough (Figure 1).

2. Samples and Methods

Over the last few years several voyages on the R/V *Tangaroa* have collected hydrographic data, surface sediment samples, piston and gravity cores (A. Rowden, TAN0803 – Macquarie Ridge 2, Unpublished RV Tangaroa Voyage report. National Institute of Water and Atmospheric Research, New Zealand, 2008; H. C. Bostock, TAN1106 – Solander Trough, 10th April - 1st May 2011. Unpublished RV Tangaroa Voyage Report, National Institute of Water and Atmospheric Research, Wellington, New Zealand, 2011), with the aim of understanding modern [*Smith et al*., 2013] and past changes in the S-STF south of New Zealand. This paper uses 20 core tops/surface samples (top 2 cm) from the Solander Trough/Emerald Basin region and then focuses on the down core data from four cores along a roughly north-south transect, ~1° latitude apart, from the Solander Trough. These are compared to a core from the northwest Campbell Plateau (Figure 1b and Tables 1 and 2). The latter core was included in this study as previous work on cores from the Campbell Plateau using stable isotopes from planktic foraminifera has suggested that this area remained covered by SAW throughout the last 130 ka due to the topographic constraint on the S-STF and SAF [*Neil et al*., 2004]. Here we provide new paleo-SST estimates from foraminiferal assemblages from the Campbell Plateau to provide an SAW end-member to compare with the paleo-SST results from the Solander Trough cores.

The top 2 m of the cores were subsampled at 5 or 10 cm intervals. The samples were dried at 50°C and disaggregated by soaking in a buffered washing solution, then wet sieved to separate the >63 μm fraction. The carbonate content was determined using the gasometric quantitative analysis after acidification with a precision of ±2% [*Jones and Kaiteris*, 1983; *Neil et al*., 2004].

Stable isotopes were measured on planktic foraminifera *Globigerina bulloides* picked from the 200–350 μm size fraction and analyzed on the Finnigan MAT 252 at the National Institute of Water and Atmospheric Research, Wellington, New Zealand, following the methods of *Neil et al*. [2004]. Radiocarbon dates were undertaken at key depths down the cores to complement the oxygen isotope stratigraphy. Between 4–10 mg of mixed planktic foraminifera were used for the ^{14}C AMS date. The dates were calibrated using CALIB 7.0 [*Stuiver and Reimer*, 1993], using Marine13 calibration and a modeled local reservoir age of 400 yrs ($\Delta R = 0$ [*Butzin et al*., 2005]). This reservoir age is similar to the average of the 10 nearest measured reservoir ages around coastal New Zealand [*Rafter et al*., 1972; *Higham and Hogg*, 1995]. We assume that the reservoir age has remained constant since the last glacial as we have no other independent age control.

The planktic foraminiferal census counts were undertaken on core tops and down cores at 5 or 10 cm intervals. Species census counts of ~200 individuals were made from a microsplit of the >150 μm size fraction at Geomarine Research, Auckland, New Zealand. Dissolution was checked by calculating the foraminiferal fragmentation using the method of *Le and Shackleton* [1992]. Foraminiferal assemblages can be affected by secondary processes including dissolution or transport. Several of the cores/surface samples sit below the current calcite saturation horizon at ~3100 m (Bostock et al., unpublished report, 2011; Table 2); however, little fragmentation is recorded in the samples with the foraminiferal fragmentation index <10% throughout (not shown). Only one core top showed significant fragmentation and evidence of dissolution (TAN1106-49; 4267 m). Thus, we assume that dissolution did not affect the majority of the planktic foraminiferal assemblages. However, we cannot discount lateral transport down the trough or vertical displacement from the sides of the trough affecting some of the samples, as is evident in benthic foraminiferal assemblages from the Solander Trough core tops [*Hayward et al*., 2013].

Mean annual SST was predicted from the planktic foraminiferal census data applied to models which used the SH0911C2 Southern Hemisphere core top training set [*Cortese et al*., 2013] targeted on mean annual SST from CARS (2009). Estimates using the modern analogue technique (MAT) [*Hutson*, 1980] were

Table 1. List of Cores in the SW Pacific (Shown on Figure 1a)[a]

Core	Latitude	Longitude	Overlying Water Mass	Proxy	Glacial Water Mass	Reference
MD03-2611	36.733°S	136.550°E	STW	Alkenones, foraminiferal assemblage, stable isotopes	SAW	*Calvo et al.* [2007], *Moros et al.* [2009], and *De Deckker et al.* [2012]
E55-6	38.853°S	141.050°E	STW	Foraminiferal assemblages, stable isotopes	STW	*Passlow et al.* [1997]
RS067-GC10	38.860°S	140.100°E	STW	Foraminiferal assemblages, stable isotopes	STW	*Passlow et al.* [1997]
MD97-2121	40.382°S	177.995°E	STW	Foraminiferal assemblages, stable isotopes, alkenones, Mg/Ca *G. bulloides* and *G. ruber*	STW/incursions of SAW	*Carter and Manighetti* [2006], *Pahnke and Sachs* [2006], *Carter et al.* [2008], and *Marr et al.* [2013]
P69	40.397°S	178.000°E	STW	Foraminiferal assemblages, stable isotopes	STW/incursions of SAW	*Weaver et al.* [1998] and *Nelson et al.* [2000]
CHAT-1 K	41.580°S	171.500°W	STW	Foraminiferal assemblages, stable isotopes	STW	*Weaver et al.* [1998]
ODP1123	41.786°S	171.499°W	STW	Foraminiferal assemblages, stable isotopes	STW/ incursions of SAW	*Crundwell et al.* [2008], *Hayward et al.* [2008], and *Lüer et al.* [2008a]
SO136-GC3	42.300°S	169.883°E	STW	Alkenones, foraminifera assemblage, stable isotopes	STFZ	*Pelejero et al.* [2006] and *Barrows et al.* [2007]
R657	42.533°S	178.493°W	STW	Stable isotopes, foraminiferal assemblages, alkenones	STW	*Weaver et al.* [1998] and *Sikes et al.* [2002]
ODP1125	42.550°S	178.167°W	STW	Foraminiferal assemblages	STW	*Schaefer et al.* [2005] and *Hayward et al.* [2008]
W268	42.851°S	178.969°E	STW	Stable isotopes, foraminiferal assemblages, alkenones	STW	*Sikes et al.* [2002]
SO136-GC11	43.440°S	167.851°E	STW	Alkenones, stable isotopes	SAW	*Barrows et al.* [2007]
MD06-2986	43.449°S	167.900°E	STW	Foraminiferal assemblages, stable isotopes	SAW	*Hayward et al.* [2012]
FR1/94-GC03	44.260°S	150.000°E	STFZ	Alkenones, stable isotopes, foraminiferal assemblages	SAW	*Barrows et al.* [2000], *Calvo et al.* [2004], and *Pelejero et al.* [2006]
U939	44.494°S	179.501°E	STFZ/SAW	Stable isotopes, foraminiferal assemblages, alkenones	SAW	*Weaver et al.* [1998], *Sikes et al.* [2000], and *Sikes et al.* [2002]
RS147-GC31	44.533°S	149.050°E	STFZ	Stable isotopes, foraminiferal assemblages, alkenones	SAW	*Sikes et al.* [2009]
ODP 1119	44.756°S	172.393°E	STFZ	Stable isotopes, foraminiferal assemblages	SAW	*Wilson et al.* [2005] and *Hayward et al.* [2008]
E27-30	45.067°S	147.228°E	STFZ	Foraminiferal assemblages, stable isotopes	SAW	*Passlow et al.* [1997]
U938	45.075°S	179.499°E	SAW	Foraminiferal assemblages, stable isotopes, alkenones	SAW	*Weaver et al.* [1998], *Sikes et al.* [2000], and *Sikes et al.* [2002]
RS147-GC07	45.150°S	146.283°E	STFZ	Foraminiferal assemblages, stable isotopes, alkenones	SAW	*Sikes et al.* [2009]
DSDP 594	45.524°S	174.948°E	SAW	Foraminiferal assemblages, stable isotopes	SAW	*Nelson et al.* [1993], *Martinez* [1994], *Weaver et al.* [1998], and *Hayward et al.* [2008]
MD97-2120	45.534°S	174.931°E	SAW	Stable isotopes, Mg/Ca *G. bulloides*, alkenones	SAW	*Pahnke et al.* [2003], *Pahnke and Zahn* [2005], and *Pahnke and Sachs* [2006]
Q200	46.000°S	172.000°E	STFZ/SAW	Foraminiferal assemblages, stable isotopes	SAW	*Weaver et al.* [1998]
RS147-GC14	46.433°S	145.233°E	STFZ	Foraminiferal assemblages, alkenones, stable isotopes	SAW	*Sikes et al.* [2009]
Y8	46.975°S	178.656°W	SAW	Radiolarian assemblages, stable isotopes	SAW	*Lüer et al.* [2008b]
TAN0803-09	46.997°S	166.061°E	STFZ	Foraminiferal assemblages, stable isotopes	SAW	This study
RS147-GC17	47.750°S	145.817°E	SAW	Foraminiferal assemblages, alkenones, stable isotopes	SAW	*Sikes et al.* [2009]
TAN1106-89	47.971°S	169.360°E	STFZ/SAW	Foraminiferal assemblages, stable isotopes	SAW	This study
TAN1106-28	48.372°S	165.659°E	STFZ	Foraminiferal assemblages, stable isotopes	SAW	This study
TAN1106-34	49.302°S	165.166°E	STFZ	Foraminiferal assemblages, stable isotopes	SAW	This study
TAN1106-43	50.449°S	164.878°E	SAW	Foraminiferal assemblages, stable isotopes	SAW	This study

[a]The overlying modern water mass and the interpreted glacial water mass from SST are shown. STW: Subtropical waters, STFZ: Subtropical frontal zone waters, and SAW: Subantarctic waters.

Table 2. Location of Cores and Core Tops/Surface Samples Used in This Study (Figures 1b and 2)[a]

Station	Core Top Number	Latitude (°S)	Longitude (°E)	Water Depth (m)	Overlying Water Mass[b]	Mean Annual SST (°C)
A830	1	46.708	167.083	476	STFZ	13.4
E824	2	46.975	166.547	1217	STFZ	13.0
TAN0803-09	3	46.997	166.061	1650	STFZ	12.8
TAN1106-16	4	47.340	165.791	1120	STFZ	12.4
A847	5	47.450	166.783	909	STFZ	12.7
TAN1106-22	6	47.593	165.239	3659	STFZ	11.6
TAN1106-89 (Campbell Plateau)		**47.971**	**169.360**	**671**	**SAW**	**10.1**
TAN1106-75 Trigger core	7	47.973	165.784	2903	STFZ	12.0
TAN1106-26, 0–2 cm	8	47.984	165.783	2840	STFZ	12.0
TAN1106-28	9	48.372	165.659	2798	STFZ	11.2
TAN0803-24	10	48.797	165.296	2962	STFZ	10.5
TAN1106-34	11	49.302	165.166	3416	STFZ	9.8
TAN0803-27, 1–2 cm	12	49.524	164.609	3250	STFZ/SAW	9.7
TAN1106-38	13	49.693	165.075	3614	STFZ/SAW	9.9
TAN0803-40, 1–2 cm	14	50.432	164.2865	3524	SAW	9.2
TAN1106-43	15	50.449	164.878	3670	SAW	9.4
D169	16	50.792	163.958	896	SAW	8.9
TAN1106-47	17	51.266	165.040	3816	SAW	9.0
TAN1106-49	18	51.568	164.657	4267	SAW	8.9
TAN0803-127	19	57.555	160.875	3830	AASW	2.8
TAN0803-124	20	58.667	160.220	4358	AASW	2.9

[a]Core highlighted in bold is from the Campbell Plateau, not from the Solander Trough, and is not used in the transection in Figure 2.
[b]Modern overlying water mass and mean annual SST (CARS, 2009).

made with the rioja package (http://cran.r-project.org/web/packages/rioja/index.html). Results from this nearest neighbor strategy were compared with those from a tree-based regression method, Random Forests (RF) [*Breiman*, 2001] using the randomForest package (http://cran.r-project.org/web/packages/randomForest/index.html). Regression error characteristic curves [*Bi and Bennett*, 2003] indicate that MAT outperforms RF over most of the range. This is supported by the Solander Trough core top data, which show a good agreement between the modern mean annual SST (CARS 2009) and the estimated SST for MAT ($R^2 = 0.72$, error of ±2°C and standard deviation of 1.4) and for RF ($R^2 = 0.62$, ±2.4°C, standard deviation of 1.5; Figure 2c).

As another alternative SST estimate we used the previously determined relationship between summer SST (SSST; between 3 and 11°C) and % *Neogloboquadrina pachyderma* (>6%) developed from 245 Southern Ocean core tops [*Govin et al*., 2009].

$$\mathrm{SSST} = -0.087 \times \%\, N.\ pachyderma + 11.339\ R^2 = 0.72.$$

This relationship has been used to estimate past SSST from cores in the Indian [*Govin et al*., 2009] and Atlantic sectors [*Vázquez Riveiros et al*., 2010] of the Southern Ocean. We find a relatively good agreement between the mean SSST overlying the Solander Trough core tops (CARS, 2009) and the SSST estimated by the % *N. pachyderma* ($R^2 = 0.61$, ±2°C, standard deviation of 1.6; Figure 2c).

3. Results

3.1. Core Tops

3.1.1. Foraminiferal Assemblages and SST Estimates

The foraminiferal assemblages in the core tops are dominated by five species: *G. bulloides*, *Globorotalia inflata*, *Neogloboquadrina incompta*, *Globorotalia truncatulinoides* (sinistral coiling), and *Neogloboquadrina pachyderma*. The 20 core tops from >400 m water depth within the Solander Trough and further south into the Emerald Basin display changes in the planktic assemblage with latitude and overlying surface waters (Tables 2 and 3 and Figure 2a). Unfortunately, there are no core top samples available south of the N-SAF and north of the N-PF in the Emerald Basin as the strong bottom currents of the ACC have removed most of the sediment in this region [*Carter and McCave*, 1997] (Figure 1b).

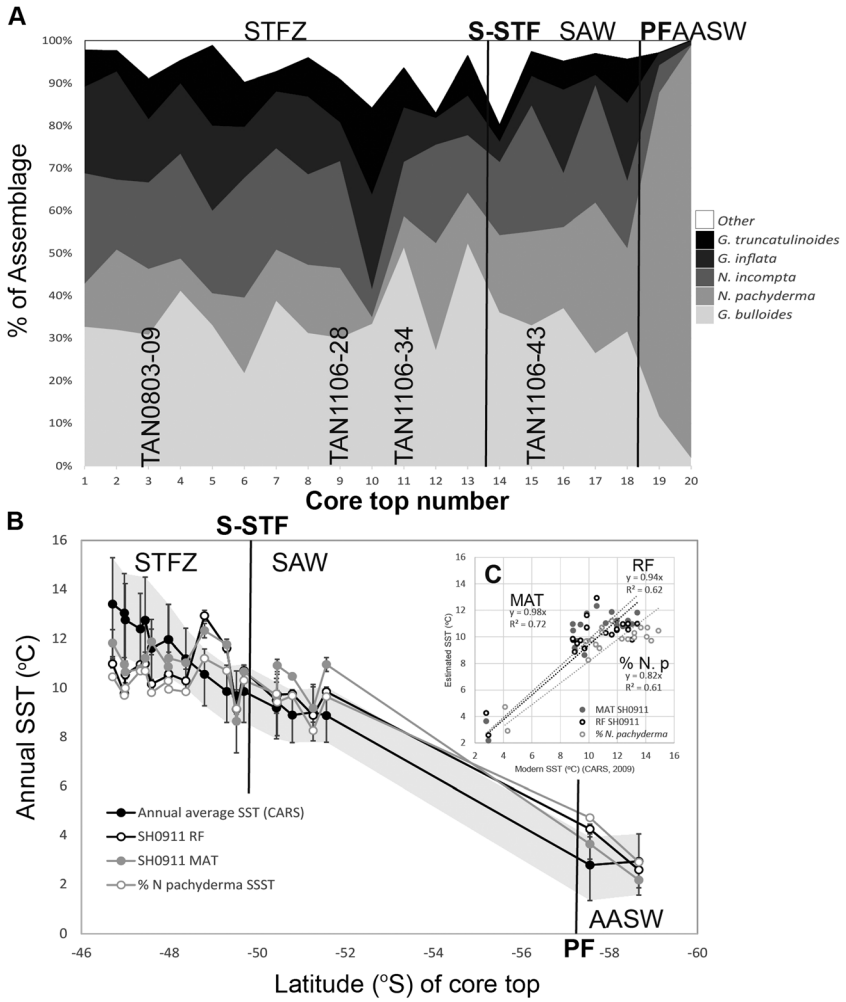

Figure 2. Core top foraminiferal assemblages from Solander Trough (core top numbers from Table 2) with the location of the main water masses and fronts from the modern oceanography highlighted; STFZ:Subtropical Frontal Zone, S-STF: Southern Subtropical Front, SAW: Subantarctic Waters, PF: Polar Front, AASW: Antarctic Surface Waters. (a) The % of the predominant foraminifera, (b) the Annual mean SST (CARS, 2009; with annual range shown by the error bars and highlighted in gray), and the estimated SST from the foraminiferal assemblages in the core tops using the different methods; Modern Analogue Technique (MAT; with error bars to show the minimum and maximum of the three nearest core top analogues); Random Forest (RF; with error bars highlighting the standard errors) and % *N. pachyderma*. (C) Comparison of the modern SST and the estimated SST from MAT, RF, and % *N. pachyderma*. All three methods have an $R^2 > 0.6$.

North of the S-STF the foraminiferal assemblage is made up of *G. bulloides*, followed by *N. incompta*, *G. inflata*, and *N. pachyderma* (Table 3 and Figure 2a). These are considered a subpolar assemblage, accompanied by the presence of *G. inflata*, which is considered to be more typical of a transitional assemblage [*Molfino et al.*, 1982; *Weaver et al.*, 1997]. In the core tops directly under the S-STF, the assemblage is dominated by the eutrophic

Table 3. Average Relative Abundance (and Range) of Common Planktic Foraminifera in Solander Trough Core Tops >400 m Water Depth

Species	North of S-STF	S-STF	South of S-STF (SAW/CSW)	South of PF
G. bulloides	32% (21–40%)	45% (27–52%)	33% (26–37%)	6% (2–12%)
G. inflata	17% (9–25%)	11% (6–16%)	10% (2–19%)	2% (1–3%)
N. incompta	21% (16–28%)	14% (6–23%)	21% (12–27%)	3% (0–6.5%)
G. truncatulinoides	10% (5–20%)	7% (1–9%)	6% (3–10%)	0% (0%)
N. pachyderma	12% (7–19%)	14% (7–25%)	23% (18–35%)	86% (76–97%)

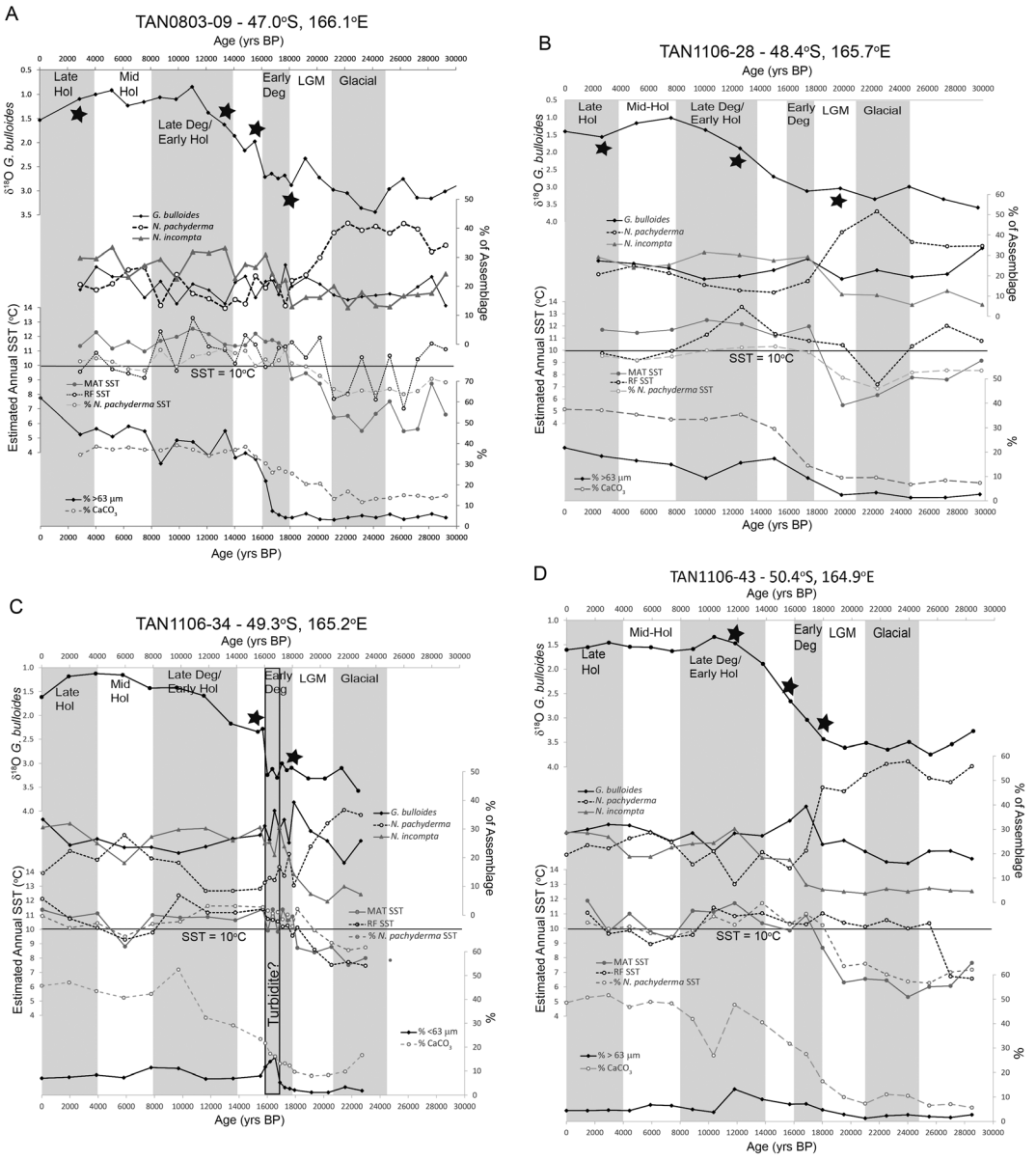

Figure 3. Down core δ^{18}O *G. bulloides*, % of the main foraminifera in the assemblage, estimated paleo-SST using MAT, RF (error bars same as Figure 2b), and % *N. pachyderma*, % $CaCO_3$, and % >63 μm (sand content) for (a) TAN0803-09, B) TAN1106-28, (c) TAN1106-34, (d) TAN1106-43, and (e) TAN1106-89. The six time slice glacial period (25–21 ka), LGM (21–18 ka), early deglacial period (18–16 ka), late deglacial/early Holocene period (14–8 ka), mid-Holocene period (8–4 ka), and late Holocene period (4–0 ka) are highlighted. The stars show the radiocarbon dates for each of the cores. The 10°C isotherm is shown by a black line.

species *G. bulloides*, with an average of 45%, the largest abundance across the region (Table 3 and Figure 2a). This may be due to the increased productivity along the front [*Crundwell et al.*, 2008; *Scott*, 2013]. To the south of the S-STF in the Solander Trough the planktic assemblages are still dominated by *G. bulloides*, but *N. pachyderma* is the second most common species along with *N. incompta* (Table 3 and Figure 2a). Thus, this would still be considered a eutrophic-subpolar assemblage [*Weaver et al.*, 1997]. South of the PF the assemblage changes dramatically and is dominated by *N. pachyderma* (>70%)—a typical polar/subantarctic assemblage [*Morigi et al.*, 2003].

There is generally good agreement between the core top foraminiferal assemblage SST estimates from the different statistical and empirical methods. However, all the methods consistently underestimate the annual SST north of the S-STF and slightly overestimate SST south of the front (Figure 2b). The former is most likely

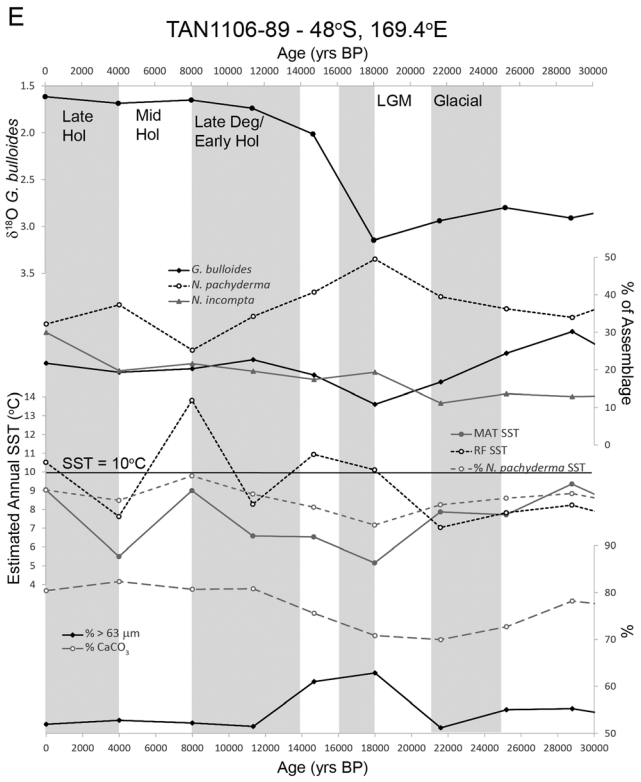

Figure 3. (continued)

due to the fact that other environmental factors also influence the foraminiferal assemblages in this region such as primary productivity [*Scott*, 2013] or neritic shelf waters [*Smith et al.*, 2013], or mixing of water masses and eddy activity. The latter overestimate of SSTs south of the front is probably related to the fact that foraminifera in the cooler SAW are productive only during the warmer months [*Northcote and Neil*, 2005].

3.2. Down Core

3.2.1. Stable Isotopes, Chronology, and Sedimentation Rates

The oxygen stable isotopes ($\delta^{18}O$) analyzed on planktic foraminiferal species *G. bulloides* show a deglacial signature decreasing from a maximum of 2.5–3.5‰ at the LGM (~18 ka) to 1–1.5‰ during the Holocene (Figure 3). These provided the initial chronology, which was then complemented by up to four radiocarbon ages on mixed planktic foraminifera per core (Table 4). The linear sedimentation rates for the cores vary from 2 cm/kyr for the Campbell Plateau core TAN1106-89 to an average 4 cm/kyr for TAN1106-28 and between 5 and 10 cm/kyr for TAN0803-09 and TAN1106-43. TAN1106-34 displays very high sedimentation rates during the early deglacial at ~28 cm/kyr. This is possibly the result of a turbidite (see more detail below).

3.2.2. Carbonate and Grain Size

The sediment in the Solander Trough cores is hemipelagic with a large proportion of terrigenous material, compared to the Campbell Plateau core, TAN1106-89 (Figure 3e). None of the cores presented here display visual evidence of turbidites in the top 2 m of the core. However, there was a small peak in the >63 µm fraction in the early deglacial period in TAN1106-34, which reached 15%, while there was no coeval increase in $CaCO_3$%. There were very high linear sedimentation rates, which suggest that this section may have been influenced by a turbidite (Figure 3c). In general, terrigenous material dominated during the glacial, when carbonate content was around 5–15%. Carbonate content increased at the start of the deglacial reaching 30–50% during the Holocene. The sand fraction (>63 µm) was around 5% for the glacial in all cores and increased to as much as 60% in the northernmost core during the Holocene but remained low at around 5% for the distal southern cores. In contrast the core from the Campbell Plateau was dominated by carbonate sediments with 60–80% carbonate and 40–60% sand similar to previous cores from this region (Figure 3e) [*Neil et al.*, 2004]. There are only minor amounts of opal present in the cores (not shown, but a few radiolarian and diatoms were visible in southern cores under the microscope).

Table 4. Radiocarbon Ages and Calibrated Ages From the Cores Analyzed on Mixed Planktic Foraminifera

Core	Depth	Laboratory Number	Conventional Radiocarbon Age and Error	Calibrated Age Range (2 sigma) yr B.P. ($\Delta R = 0$ [*Butzin et al.*, 2005])
TAN0803-09	5–6 cm	NZA 30754	3,059 ± 40	2,739–2,930
	50–51 cm	NZA 54362	11,798 ± 33	13,174–13,373
	70–71 cm	NZA 30246	13,600 ± 60	15,653–16,073
	90–91 cm	NZA 54363	15,286 ± 46	17,918–18,268
TAN1106-28	10–11 cm	NZA 54355	2,860 ± 18	2,532–2,715
	50–51 cm	NZA 54358	10,972 ± 31	12,443–12,630
	80–81 cm	NZA 54357	16,716 ± 53	19,515–19,909
TAN1106-34	80–81 cm	NZA 54364	13,339 ± 37	15,263–15,654
	150–151 cm	NZA 54356	15,112 ± 44	17,722–18,053
TAN1106-43	80–81 cm	NZA 54359	10,540 ± 30	11,546–11,997
	100–101 cm	NZA 54360	13,463 ± 37	15,404–15,844
	120–121 cm	NZA 54361	15,155 ± 43	17,782–18,108

3.2.3. Foraminiferal Assemblages and Paleo-SST

North of the modern S-STF the Holocene foraminiferal assemblages was similar to the core tops (Figures 2 and 3 and Table 3) but with fewer *G. bulloides* and more *N. incompta*. While in TAN1106-43, south of the S-STF, the Holocene foraminiferal assemblages had more *N. incompta* than the core top (Figure 3d). The Campbell Plateau core TAN1106-89 had more *N. pachyderma* and less *N. incompta* and *G. bulloides* (Figure 3e). The glacial assemblages in all five of the cores are considerably different with a higher % of *N. pachyderma* in most of the cores and a reduction in the abundance of *N. incompta* (Figure 3).

During the glacial period the MAT SST sat between 5.5 and 9°C in all the cores (Table 5, Figures 3a–3e, and Figure 4). The RF SST estimates tend to be higher than the MAT SST (Figures 3a–3e). The biggest difference between the MAT and RF SST is in core TAN1106-43, where the RF SST increased significantly earlier in the glacial period than the change in MAT SST (Figure 3d). This appears to be the result of a couple of rare specimens of juvenile *G. sacculifer*, possibly misidentified in these samples, which has a strong control on the RF SST estimates [*Cortese et al.*, 2013]. Thus, the majority of our interpretation of the cores will be based on the MAT SST estimates.

All the Solander Trough cores show a dramatic warming in MAT SST of 3–5°C during the deglacial period (Figures 3a–3d and Figure 4). The timing of this change was different between the cores, with TAN0803-09 and TAN1106-34 displaying an increase in SST prior to the end of the LGM (Figure 4). High SSTs are found in the late deglacial/early Holocene periods in cores TAN1106-28, TAN1106-34, and TAN1106-43. During the mid-Holocene period there was a dip in SST in TAN1106-34 and TAN1106-43, before a slight recovery in SST in the late Holocene period (Table 5 and Figure 4).

In the paleoceanography literature there have been two approaches to reconstructing the position of the S-STF [*Kohfeld et al.*, 2013]. One approach has been to tie a front to a single isotherm (e.g., 10°C). However, the modern S-STF does not sit at the same isotherm throughout the Southern Hemisphere. The second, and more robust approach used by oceanographers in the modern ocean, is to use the SST gradients between sites.

Table 5. MAT SST From Each Core for Different Time Slices and the Modern SST From CARS (2009)[a]

Cores	Glacial (25–21 ka)	LGM (21–18 ka)	Early Deglacial (18–16 ka)	Late Deglacial/ Early Holocene (14–8 ka)	Mid-Holocene (8–4 ka)	Late Holocene (4–0 ka)	Modern (CARS 2009)
TAN0803-09 47°S	*5.5–7.5*°C	***8.9–10.2*°C**	**11–12°C**	**11.3–12.5°C**	**11–12°C**	**11.3–12.3°C**	**12.76°C**
TAN1106-28 48.4°S	*6.3–8.6*°C	*5.5*°C	**11.2–12°C**	**11.2–12.4°C**	**11.4–11.7°C**	**11.4–11.7°C**	**11.18°C**
TAN1106-34 49.3°S	*7.5–7.8*°C	*8.4–8.8*°C	***9.9–11.4*°C**	**10.3–10.9°C**	***9.8–11.1*°C**	**10.8–11.4°C**	***9.85*°C**
TAN1106-43 50.4°S	*5.3–7.7*°C	*6.3–6.9*°C	*8.5*°C	***10.2–11.4*°C**	*8.5–9.4*°C	***9.8–11.9*°C**	*9.41*°C
TAN1106-89 48°S (Campbell)	*7.8–8.9*°C	*5.2*°C	*6.5*°C	*6.5–10.4*°C	*5.5*°C	*9*°C	***10.11*°C**

[a]Assuming the 10°C isotherm represents the S-STF. The values in italics represent SAW, while the bold ones represent STFZ. Values in bold and italics suggest that the cores sit under or in close proximity to the S-STF.

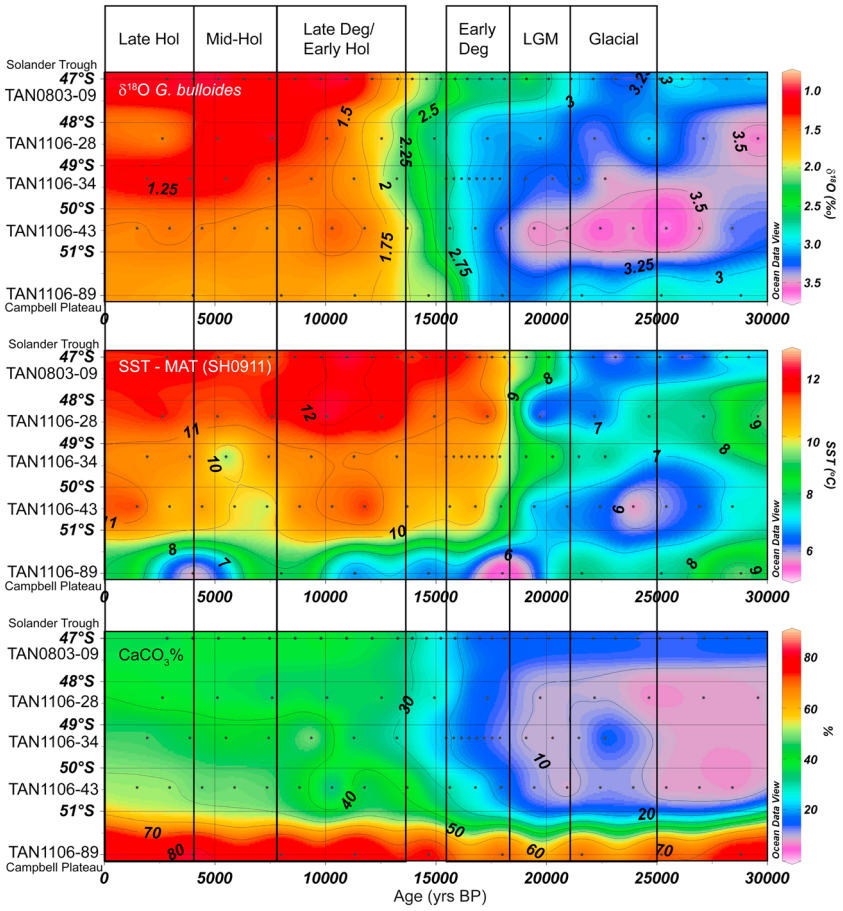

Figure 4. Latitudinal and age plots of δ^{18}O *G. bulloides*, estimated paleo-SST using MAT (SH0911) and % $CaCO_3$. The data from the Campbell Plateau core are also shown at the bottom of each stack in oceanographic order (rather than latitudinal order). The color bars and contours show the data values. The six time slices are highlighted outlined in the text and caption for Figure 3. Plot created using Ocean Data View [*Schlitzer*, 2009].

These two methods are illustrated in Tables 5 and 6 with the locations of the fronts highlighted for the six time slices. The SST gradients between the four cores in the Solander Trough were calculated using the average MAT ΔSST between cores, then dividing by the distance in kilometers between the core locations (Table 6). Values of >1°C/100 km were considered evidence for a front [*Graham and De Boer*, 2013; *Smith et al*., 2013]. The results suggest that there were steep SST gradients during the LGM and early deglaciation (>1°C/100 km [*Graham and De Boer*, 2013]), but these decreased in the Holocene period with maximum SST gradients ~1°C/100 km. The underestimation of the warmer temperatures and the overestimation of the cooler temperatures using the MAT technique suggest that the calculated SST gradients are likely to be an underestimate, especially as temperatures increased (>11°C; Figure 2b) in the late deglacial and Holocene periods.

Table 6. SST Gradients Between the Different Core Locations for Different Time Slices and the Modern Gradient From CARS (2009)[a]

SST Gradients (°C/100 km) ΔSST	Glacial (21–25 ka)	LGM (21–18 ka)	Early Deglacial (18–16 ka)	Late Deglacial/Early Holocene (14–8 ka	Mid-Holocene (8–4 ka)	Late Holocene (4–0 ka)	Modern (CARS, 2009)
47–48.4°S 173 km	0.55 (−0.95)	**2.34 (4.05)**[b]	−0.06 (−0.1)	0.06 (0.1)	−0.03 (−0.05)	0.14 (0.24)	0.84 (1.28)
48.4–49.3°S 115 km	0.17 (−0.2)	−2.69 (−3.1)	0.83 (0.95)	*1.04 (1.2)*[b]	0.95 (1.1)	0.41 (0.47)	*1.05 (1.22)*[b]
49.3–50.4°S 150 km	−0.77 (1.15)	*1.33 (2)*[b]	**1.43 (2.15)**[b]	−0.13 (−0.2)	*1 (1.5)*[b]	0.18 (0.27)	0.35 (0.52)
50.4–48°S (Campbell)	(−1.65)	(1.4)	(2)	(2.35)	(3.5)	(1.82)	(−0.85)

[a]Shown are the SST gradients (°C/100 km) and average temperature differences (ΔSST in brackets) between adjacent cores.
[b]The largest SST gradients are in bold and italics. During the LGM and early deglacial there are strong S-STF fronts in the Solander Trough (>1.25°C/100 km; in bold), while during the Holocene and modern there are only weaker S-STF fronts (~1°C/100 km; in italics) fluctuating between 48.4 and 50.4°S.

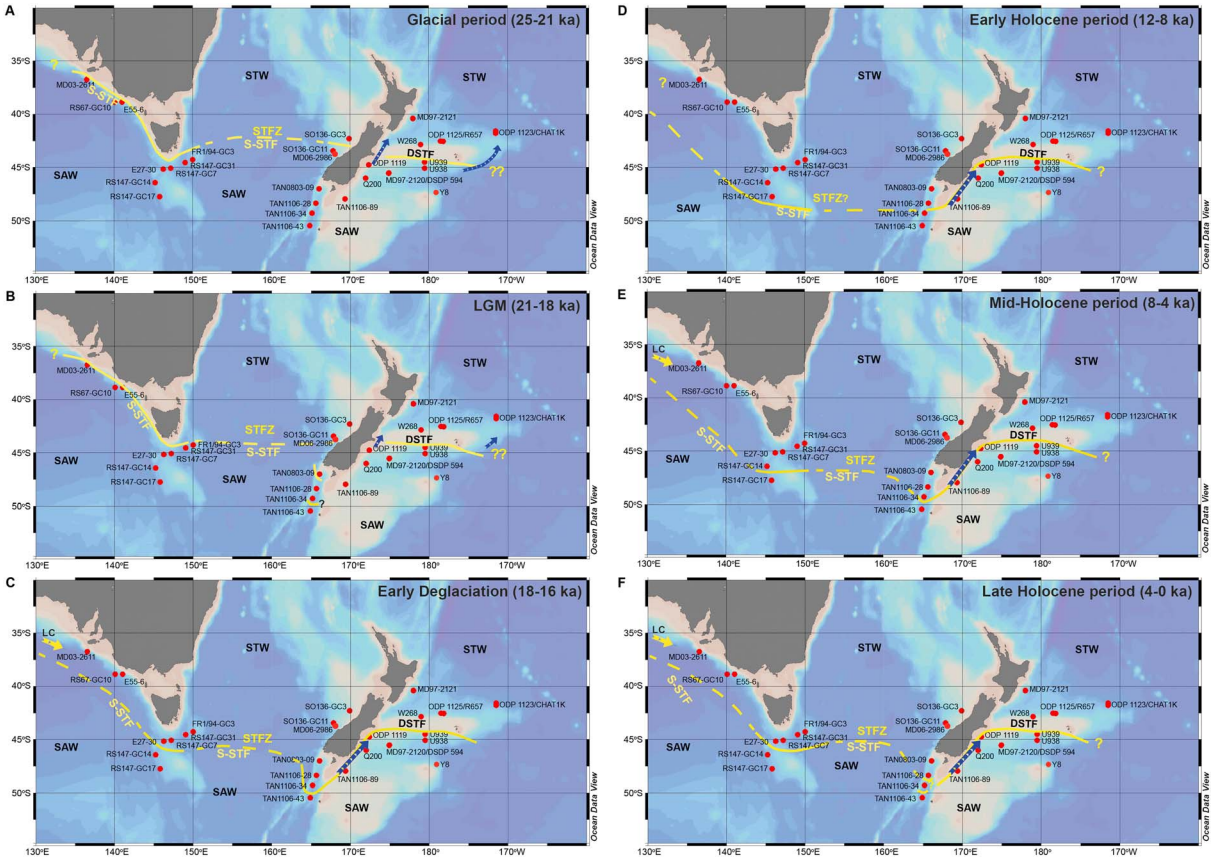

Figure 5. Reconstruction of the Southern Subtropical Front–S-STF (yellow line) and Dynamical Subtropical Front–DSTF for the southwest Pacific Ocean. The dashed yellow line indicates regions where there are no cores to constrain the location of the S-STF. STW: Subtropical Water, SAW: Subantarctic Water. (a) Glacial period (25–21 ka), (b) LGM: Last Glacial Maximum (21–18 ka), (c) early deglaciation (18–16 ka), (d) early Holocene period (12–8 ka), (e) mid-Holocene period (8–4 ka), (f) late Holocene period (4–0 ka). Core locations from Table 1 are shown by red dots. The blue arrows show SAW flowing north of the S-STF during the glacial period and LGM.

4. Discussion

4.1. Changes in the Position of the S-STF South of New Zealand

For the glacial period (25–21 ka) the foraminiferal assemblage paleo-SST estimates suggest that the SSTs for all the Solander cores were significantly lower (5–9°C) than the modern mean annual SST (9–13°C) and similar to the Campbell Plateau SST (7–9°C; Table 5 and Figure 4). The SST gradient was very small (≪1°C/100 km) between the Solander Trough cores at this time (Table 6 and Figure 4). This suggests that the S-STF had most likely moved at least 2° equatorward of its modern position as there is no evidence for the S-STF south of New Zealand during the glacial period (Figures 4 and 5a). During this time the whole Solander Trough region was overlain by cool SAW.

During the LGM (21–18 ka), SST started to increase at the northernmost core TAN0803-09 (47°S) at ~20 ka (Figure 4 and Table 5), while most of the cores further south remained cold (5–8°C). There is also evidence for early warming at TAN1106-34 (49.3°S) during the LGM (Figure 4), but there may be some issues with the age model of this core. The steepest SST gradient at this time was between 47 and 48.4°S (>2°C/100 km; Table 6), which is twice the modern gradient across the S-STF. This suggests that the S-STF had shifted south of New Zealand (Figure 5b). A second strong SST gradient (>1°C/100 km) also existed between the cores at 49.3°S and 50.4°S. This may be due to the age model (as explained above), or a second weaker front further south, similar to the modern situation [*Smith et al.*, 2013]. However, SST in TAN0803-09 had barely reached 10°C and the SST MAT estimates for the other cores were <10°C (Figures 3a and 4), indicating that the temperatures at the front were cooler than the modern S-STF conditions.

Farther south the SST dramatically increased at the onset of the deglaciation (18 ka; Figure 4). However, the SST in the southern-most core was a little more sluggish and only reached a peak in SST around 15 ka (Figures 3d and 4). Thus, in both the isotherm and SST gradient methods (>1.4°C/100 km) the early deglaciation S-STF sat between 49.3°S and 50.4°S (Tables 5 and 6 and Figure 5c). During the early deglaciation the SST increase in all the cores led the decrease in δ^{18}O *G. bulloides* and the increase in carbonate and sand content by ~2000 years (Figure 4), a phenomenon that has also been observed previously in other cores in this region [*Barrows and Juggins*, 2005].

In the late deglaciation/early Holocene period (14–8 ka) the highest SST were reached in all the Solander Trough cores (Figures 3 and 4 and Table 5). Using the 10°C isotherm approach the S-STF would have sat south of TAN1106-43 (>50.4°S), while the Campbell Plateau was still overlain by cool SAW (Table 5). The strongest SST gradient (~1°C/100 km) calculated between the four Solander Trough cores was between 48.4 and 49.3°S (Table 6 and Figure 5d). This was a considerably reduced SST gradient compared to the LGM and early deglaciation, suggesting that the S-STF may have been a broader, more diffuse front, similar to the modern S-STF in the Solander Trough [*Smith et al*., 2013].

During the mid-Holocene period (8–4 ka) there appeared to have been an overall decrease in SST with all the cores, including the one on Campbell Plateau (TAN1106-89), exhibiting slightly lower SST (Figure 4). The southernmost Solander Trough core (TAN1106-43) exhibited an SST <10°C, suggesting that the S-STF shifted north of 50.4°S at this time (Table 5). However, an SST gradient of ~1°C/100 km was present between 48.4 and 49.3°S and between 49.3°S and 50.4°S, indicating a very wide front or a highly variable position of the S-STF during this 4 kyr period (Table 6 and Figure 5e).

In the late Holocene period the SST increased again (Figure 4). Using the 10°C isotherm definition for the S-STF the front would have sat over the southernmost Solander Trough core (TAN1106-43), while the Campbell Plateau core still remained overlain by cool SAW (Table 5). However, the SST gradients between the Solander Trough cores were all significantly <1°C/100 km, suggesting the front may have sat further south (>50.4°S; Table 6 and Figure 5f). However, the Holocene SST gradients should be interpreted with caution as the ΔSST between cores (Table 5) is significantly less than the errors for the different paleo-SST estimates (±2°C), especially at warmer SST, where they consistently underestimate the SST (>11°C; Figure 2). Higher resolution samples, or use of another SST proxy, which can estimate warmer temperatures with lower errors, such as alkenones, may provide improved estimates on the SST gradient and a more definitive location of the S-STF throughout the Holocene period.

4.2. Glacial/Interglacial Changes in the S-STF in the Southwest Pacific Ocean

These results fill in the missing gap in this region, linking the previous core records from Australia and the Tasman Sea to the core data east of New Zealand (Figure 1a and Table 1). Out of necessity we have to use a combination of the isotherm and SST gradient methods to interpret the position of the S-STF across the region, as some of the previous studies have only used a single core. We assume that the S-STF is located at the 10°C isotherm for foraminiferal assemblage SSTs (as used to interpret the Solander Trough cores in this study; Figures 6b and 6c), and as coccolithophore bloom in summer we have used the 13°C isotherm for alkenone SST (Figure 6a). We use the combination of all these data to reconstruct the likely location of the S-STF across the entire southwest Pacific.

As discussed in section 1.4, previous studies from the southwest Pacific Ocean (Table 1) suggest the S-STF was located between 3 and 5° further north during the last glacial period [*Kohfeld et al*., 2013] (where they defined the LGM as 23–19 ka). *Sikes et al*. [2009] used SST estimates from foraminiferal assemblages and alkenones and found minimal SST difference (<2°C, with both proxies) between four cores (RS147-GC7, GC31, GC14, and GC17) across the South Tasman Rise during the glacial period, suggesting that the S-STF sat north of the rise (~44°S), close to Tasmania (Figure 5a), while they suggest that the summer S-STF sat south of the cores (>47.5°S) during the early Holocene period (Figure 5d). Alkenone SST and foraminiferal assemblages from core MD03-2611 also showed cool temperatures during the glacial period (Figure 6a) and suggest the S-STF may have sat as far north as ~37°S off the South Australian Coast (Figure 5a). The SST in this core shows a dramatic change at the start of the deglaciation (~18 ka), with an increase of 4-5°C (Figure 6b) and a drop in % *N. pachyderma* [*De Deckker et al*., 2012]. This change could be due to the S-STF shifting south, allowing the warm STW and the Leeuwin Current to flow in to this region [*Calvo et al*., 2007;

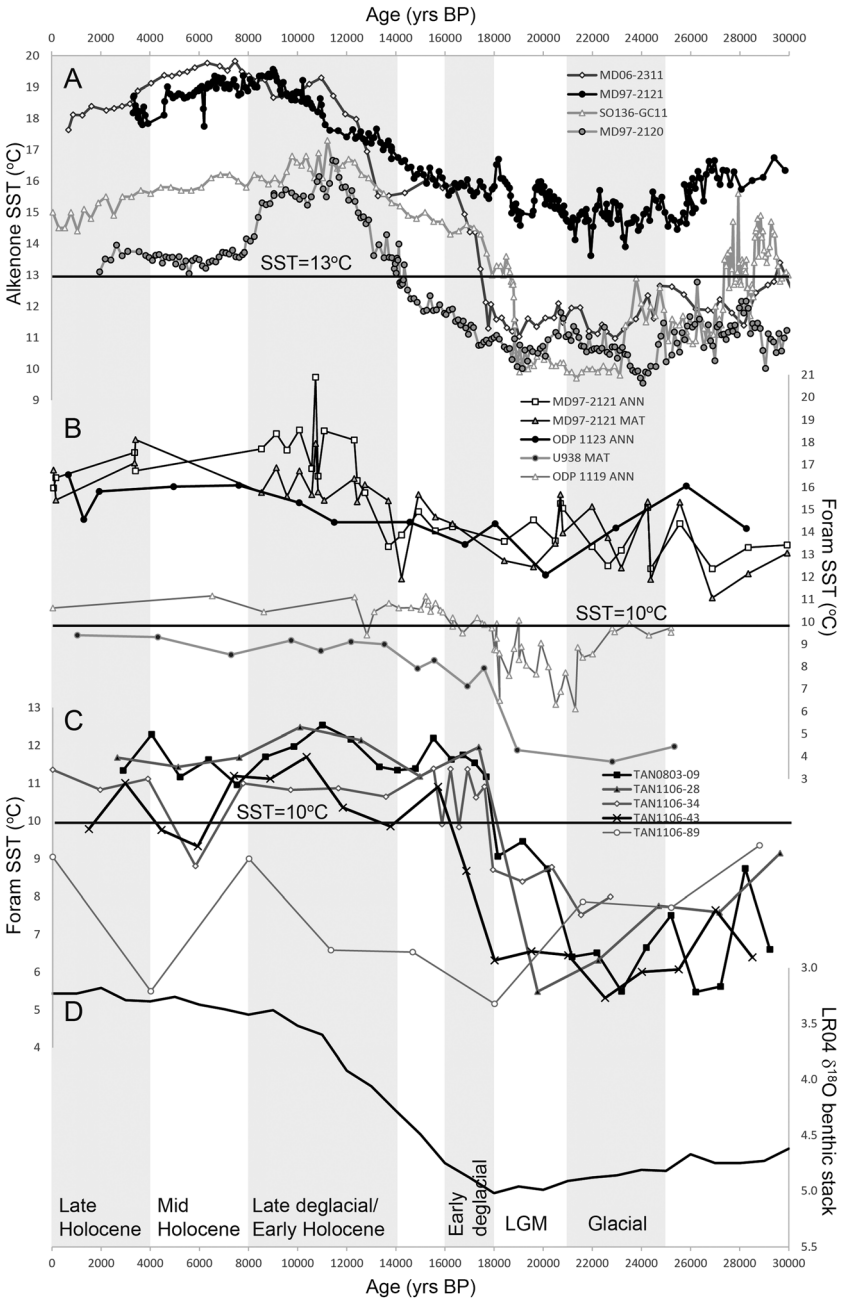

Figure 6. (a) Alkenone paleo-SST data for cores MD03-2611, South Australia [*Calvo et al.*, 2007], and SO136-GC11, west of New Zealand [*Barrows et al.*, 2007a], and MD97-2120 and MD97-2121, east of New Zealand [*Pahnke and Sachs*, 2006]. (b) Foraminiferal assemblage paleo-SST data: ODP 1123-ANN northeastern Chatham Rise [*Crundwell et al.*, 2008], MD97-2121-MAT and MD97-2121-ANN, north of Chatham Rise (unpublished) and U938-MAT [*Sikes et al.*, 2002], and ODP 1119-ANN [*Carter et al.*, 2004; *Wilson et al.*, 2005], south of Chatham Rise. (c) Foraminiferal assemblage paleo-SST data from: Solander Trough cores TAN0803-09-MAT, TAN1106-28-MAT, TAN1106-34-MAT, TAN1106-43-MAT, and TAN1106-89-MAT, Campbell Plateau (this study). (D) Global benthic foraminifera $\delta^{18}O$ stack LR04 [*Lisiecki and Raymo*, 2005], as a proxy for sea level change over the last 30 ka.

De Deckker et al., 2012] (Figure 5c). On the eastern side of the Tasman Sea foraminiferal assemblages and alkenone SST (cores SO136-GC11 (Figure 6a), GC3 and MD06-2986) showed a dramatic increase of 3–4°C in the LGM/early deglaciation (~19 ka [*Barrows et al.*, 2007a, 2007b; *Hayward et al.*, 2012]), suggested to be due to the influence of the S-STF shifting south over these core sites [*Hayward et al.*, 2012] (Figures 5b and 5c). A northward shift of the S-STF during the glacial period along the west coast of New Zealand could also

explain the equatorward bowing of the SST isotherms in this region on a map of glacial SST from foraminiferal assemblages for the southwest Pacific Ocean [*Barrows et al*., 2000; *Barrows and Juggins*, 2005].

In contrast, the glacial position of the S-STF east of New Zealand is considered to have remained locked to the Chatham Rise (~44°S) due to topographic control imposed by the shallow bathymetry (Figure 5a). SST estimates from foraminiferal assemblages in cores either side of the Chatham Rise showed a larger cooling south of the rise, leading to a greater SST difference (~8°C) across the S-STF during the glacial period (Figure 1a; R657, W268, U938, U939, CHAT 1 K, and ODP 1123; ODP 1125, and DSDP 594; and MD97-2121 and MD97-2120 [*Weaver et al*., 1998; *Sikes et al*., 2002; *Schaefer et al*., 2005; *Wilson et al*., 2005; *Hayward et al*., 2008]; some examples shown in Figure 6b). This SST difference is substantially larger than the modern SST difference across the S-STF of 4–5°C. However, there is foraminiferal assemblage evidence that cold SAW did leak north of the Chatham Rise at various times during the glacial period. At the western end of the rise SAW flowed through the Mernoo Gap supplying cold waters to the east coast of the North Island where temperatures are estimated to be 5–10°C cooler (cores P69 and MD97-2121 [*Nelson et al*., 2000; *Carter and Manighetti*, 2006; *Marr et al*., 2013]). At the eastern end of the rise there is also evidence of incursions of cooler SAW from the presence of subpolar foraminifera and radiolaria at ODP 1123 [*Crundwell et al*., 2008; *Lüer et al*., 2008a].

In contrast to the foraminiferal SST estimates, alkenone SST displayed only a 4–5°C difference across the Chatham Rise during the glacial period [*Sikes et al*., 2002; *Pahnke and Sachs*, 2006] (Figure 6a). The warmer alkenone SST estimates south of the rise, however, are not supported by coccolithophore assemblages, which suggest it was considerably cooler [*Fenner and di Stefano*, 2004] or by SST estimates from radiolarian assemblages in core Y8 on the northeastern edge of Campbell Plateau [*Lüer et al*., 2008a]. It is possible that the alkenones were responding to nutrient or light limitations [*Sikes et al*., 2005] or that the alkenone-SST calibration is not appropriate for assemblages of coccolithophores not dominated by *Emiliani huxleyi* [*Volkmann et al*., 1995] or for SST below 6°C [*Sikes and Volkman*, 1993; *Sikes et al*., 1997].

Just south of the Chatham Rise, on the continental shelf, ODP 1119 was reported as having foraminiferal assemblage SSTs of 8–10°C during the glacial and LGM periods [*Wilson et al*., 2005; *Hayward et al*., 2008] (Figure 6b). During this period a steep SST gradient (4–6°C) between site 1119 and DSDP site 594 (250 km further offshore) was inferred to indicate the presence of a front between the two sites, produced by an eastward shift of the STF/Southland Current further offshore due to the lowering of sea level (Figure 6d). Thus, core site 1119 was inferred to have been bathed in STW/STFZ waters flowing in from the south [*Carter et al*., 2004; *Hayward et al*., 2004, 2008; *Wilson et al*., 2005]. Thus, in order to link the S-STF in the Tasman Sea to the Chatham Rise it was assumed that a small amount of the S-STF must have "flowed" south around New Zealand [*Wilson et al*., 2005; *Hayward et al*., 2008].

However, revisiting the ODP 1119 SST, using the original radiocarbon data for this core [*Carter et al*., 2004], SSTs remain below 9°C between 23 and 18 ka, with the exception of 1 data point at 19 ka (Figure 6b). Thus, combining this with the results from this study, there is no evidence for the S-STF south of New Zealand during the peak glacial period and majority of the LGM (23–19 ka), and this entire region was overlain by SAW (Figures 5a and 5b). With no flow associated with the modern STFZ in the east of the Southern Hemisphere basins [*Graham and De Boer*, 2013], and the discontinuous nature of the SST gradients in the modern ocean, there is no requirement for a continuous SST front to link the S-STF on either side of the New Zealand landmass. This is the same scenario previously inferred for some of the coolest early and middle Pleistocene glacial periods [*Hayward et al*., 2008, 2012].

There was an early increase in SST (20–19 ka) in the northern Solander Trough (Figures 4 and 6c), which suggests that the S-STF shifted south and had started to influence this region prior to the end of the LGM (18 ka). There is also evidence for an early increase in SST (from multiple proxies) in several other cores around the region starting around 19 ka, including SO136-GC11 [*Barrows et al*., 2007a] and MD97-2120 [*Pahnke et al*., 2003; *Pahnke and Sachs*, 2006] (Figure 6a), and SST commonly led the oxygen isotopes in this region [*Barrows and Juggins*, 2005]. This suggests that SST led melting of the ice caps and rising global sea level and that the LGM (21–18 ka; Figure 6d) may have been more of a transitional period in this region rather than a stable cold period (Figure 5b). However, the SST warming may not be exclusively related to the S-STF shifting south as there is evidence from Antarctic ice cores

for increased atmospheric air temperatures around 19 ka [*Pedro et al*., 2011]. Modeling studies suggest that this early rise in temperatures might be the result of changes in obliquity forcing [*Roche et al*., 2011].

In the early Holocene period (12–8 ka) many of the cores adjacent to the modern S-STF, including the Solander Trough cores, exhibit a peak in SST with the warmest SST of the last 25 ka (Figures 4b and 6a). This has led to the suggestion that the S-STF was at its most southerly position at this time in the Tasman Sea [*Sikes et al*., 2009] (Figure 5d). Warm alkenone SSTs are also evident in core MD03-2611 [*Calvo et al*., 2007] (Figure 6a). In contrast, foraminiferal evidence from this same core MD03-2611 off South Australia indicates cooler SST and has led to the suggestion that the S-STF sat further north [*Moros et al*., 2009]. However, this region off South Australia has complex currents with the warm Leeuwin Current dominating during the winter and cold water from the Southern Ocean during the summer, so this contradictory data may reflect seasonal changes in the dominant currents.

In the mid-Holocene period (8–4 ka) there were weak SST gradients and a broad S-STF in the Solander Trough. In contrast, north of the S-STF alkenone SST estimates peaked both off northwest of New Zealand in core MD97-2121 [*Pahnke and Sachs*, 2006] and south of Australia in core MD03-2611 [*Calvo et al*., 2007] (Figure 6a). To the south of the S-STF alkenone and Mg/Ca *G. bulloides* SST in the SAW both declined dramatically in MD97-2120 [*Pahnke and Sachs*, 2006] (Figure 6A) (also evident in cores U939 and U938 (not shown) [*Sikes et al*., 2002]. This was potentially the result of declining insolation at 65°S at this time [*Shevenell et al*., 2011]. In contrast, SO136-GC11 (~43°S) on the edge of the modern STFZ in the east Tasman Sea was still warm, but slowly cooling [*Barrows et al*., 2007a] (Figures 5e and 6a), possibly due to mixing of the STW, with increasing influence of cooler SAW.

4.3. Implication for the Paleo-Winds

There is considerable evidence from modern oceanographic studies for a link between the strength of western boundary currents, including the DSTF (southeast of New Zealand and along Chatham Rise), and the wind stress curl in the southwest Pacific Ocean [*Chiswell*, 1996; *Tilburg et al*., 2001; *Hill et al*., 2008; *Fernandez et al*., 2014], and by association the SHWW (which have the largest influence on the wind stress curl in the Southern Hemisphere [*Lauderdale et al*., 2013]). So what do the paleo-SST gradients and the interpreted latitudinal changes in the S-STF from the southwest Pacific Ocean potentially tell us about past changes in the SHWW, if anything?

During the LGM (21–18 ka) the SSTs in the Southern Ocean were significantly cooler with a greater sea ice extent (reviewed in *Bostock et al*. [2013]), which would have allowed the polar vortex around Antarctica to expand. However, to the north there was little change in tropical SST (reviewed in *Reeves et al*. [2013]). This would have created a stronger meridional temperature gradient and increased the wind stress curl [*Bostock et al*., 2006]. Glacial and LGM paleo-SST evidence from foraminiferal assemblages from the southwest Pacific Ocean shows a very steep SST gradient (twice the modern gradient—see sections 4.1 and 4.2) in the Solander Trough and across Chatham Rise [*Sikes et al*., 2002; *Schaefer et al*., 2005; *Hayward et al*., 2008] (Table 6 and Figure 6c), which suggests that there was a strengthened DSTF at this time and supports an increase in the average wind stress curl across the South Pacific Ocean.

This increase in the wind stress curl could have been the result of either an increase in the strength of the SHWW, or a northward shift of the SHWW, as has previously been suggested by other studies [*Sikes et al*., 2009; *Kohfeld et al*., 2013]. An alternative explanation for the increase in wind stress curl in the southwest Pacific Ocean is that the typically split subtropical (30°S) and polar (60°S) SHWW jets in this region (resulting from the warm winter SST around Australia [*Taljaard*, 1972]), merged during winter and spring. This would have produced a weak surface westerly flow over a ~20° latitudinal band between ~30°S and 50°S, rather than dominant surface westerly winds at 55–65°S, which occurs during the split subtropical and polar jets [*Taljaard*, 1972; *Bals-Elsholz et al*., 2001; *Shulmeister et al*., 2004; *Pena-Ortiz et al*., 2013; *Ummenhofer et al*., 2013]. The merging of the SHWW jets during the glacial period may be a response to the limited space available between an expanded polar vortex and the subtropical Hadley Cell or due to cooler winter SST around Australia [*Taljaard*, 1972].

In contrast, the modern relationship between the STFZ and the wind stress curl is less clear. *Graham and De Boer* [2013] suggest that the STFZ shifts seasonally in the central and eastern Southern Hemisphere ocean basins. However, in the Tasman Sea the modern STFZ does not appear to shift seasonally, despite

the absence of bathymetric control (Smith and Vennell, in review). This may also be due to the split SHWW jet structure in this region. Despite this, the paleo-SST proxies from cores west of New Zealand show a significant glacial cooling of 5–7°C [*Calvo et al*., 2007; *Barrows et al*., 2007a; *Sikes et al*., 2009], suggesting that the S-STF may have shifted north, potentially responding to a large increase in the glacial wind stress curl and/or a major change in the wind patterns in this region (e.g., a dominance of a merged jet).

Many researchers have looked to global climate models (GCMs) to test the response of SST and precipitation to changes in the position and strength of the SHWW. Unfortunately, GCMs currently do not capture the complexity of the SHWW, especially in the southwest Pacific region, and there is little consensus between the results from the six GCMs that were run for the 21 ka time slice as part of the Palaeoclimate Modelling Intercomparison Project 1 and 2 [*Rojas et al*., 2009; *Chavaillaz et al*., 2013; *Sime et al*., 2013]. Specifically, half of the GCMs exhibit a northerly shift in SHWW, while the other half a southerly shift in the SHWW [*Chavaillaz et al*., 2013]. These conflicting results have been suggested to be related to issues with the different GCMs, especially related to sea ice and changes in the thickness of the Antarctic ice sheet, which in turn affect the temperature gradients at the surface [*Kidston et al*., 2011; *Chavaillaz et al*., 2013].

While the paleo-SST data from cores in the southwest Pacific Ocean during the glacial period (25–21 ka) provide a fairly consistent picture of a northward STFZ and a stronger DSTF, results from the Holocene period are highly variable and contradictory (see sections 4.1 and 4.2) and do not agree with other regions of the Southern Ocean [*Bianchi and Gersonde*, 2004; *Moros et al*., 2009; *Lamy et al*., 2010; *Voigt et al*., 2015]. This may be due to the highly variable nature of the STFZ and the weaker SST gradients (~1°C/100 km) that are difficult to determine when there are large errors on the paleo-SST data. Alternatively, different regions of the ocean should display different responses, as ocean fronts and currents are influenced by both the bathymetry and wind [*Sallée et al*., 2008]. For example, south of New Zealand the S-STF is already forced south by the bathymetry and sits at its most southerly position in the Southern Hemisphere [*Smith et al*., 2013]. Thus, the response of the S-STF in this region to a positive Southern Annular Mode (SAM; resulting in the strengthening and shifting of the SHWW polar jet and surface winds further south [*Thompson and Wallace*, 2000]) over the last decade has been a strengthening of the fronts and currents, rather than a shift in the position [*Sallée et al*., 2008; *Fernandez et al*., 2014]. In contrast, fronts in other regions of the Southern Ocean, where there are minimal bathymetric constraints, are more strongly coupled to the SHWW and have shifted south with the positive SAM [*Sallée et al*., 2008].

Clearly more work is required to understand the relationship between the SHWW/wind stress curl and the Southern Ocean fronts and currents, which will vary from basin to basin due to variations in both the atmospheric circulation and the local bathymetry. This will allow us to better interpret past changes as well as provide improved prediction under future climate change scenarios.

5. Conclusions

We compared two different methods: (1) 10°C isotherm and (2) SST gradient, to determine the past position of the S-STF within the Solander Trough over the last 25 ka. During the LGM (21–18 ka) and early deglaciation (18–16 ka) the methods agree. However, during the late deglacial and Holocene period (14–0 ka) there are differences between the interpreted locations of the S-STF in the Solander Trough (Tables 5 and 6). This suggests that the isotherm of the S-STF may not have remained the same throughout the last 25 ka and/or the paleo-SST gradients are underestimated as the SST increased in the late deglaciation and Holocene period.

The evidence from paleo-SST gradients suggests that the S-STF did not exist south of New Zealand and there was no connection between the west and east during the glacial period. This evidence supports previous suggestions that the S-STF shifted north, except where it is bathymetrically constrained by Chatham Rise. The S-STF started to influence the Solander Trough during the LGM (20–19 ka) and then shifted south rapidly during the early deglaciation (18–16 ka) to its modern position. In the late deglaciation-Holocene period (14–0 ka) paleo-SST gradients in the Solander Trough were reduced, suggesting a broader, more diffuse S-STF similar to today (or further south). Unfortunately there was conflicting evidence from other cores in the southwest Pacific Ocean and Southern Hemisphere basins during the Holocene period, with some cores suggesting the S-STF was further north and others further south.

Increased SST gradients across the S-STF along Chatham Rise and the Solander Trough during the glacial period and LGM suggests an increase in the strength of the wind stress curl and a strengthening of the DSTF. This also resulted in a northerly shift of the S-STF/STFZ south of Australia and Tasman Sea. These changes in the wind stress curl were most likely caused by variations in the strength or position of the SHWW. However, there are multiple possibilities (northward shift, strengthening, and merging of split jets in the SHWW) that could have resulted in an increased wind stress curl in this region of complex bathymetry and atmospheric circulation.

Acknowledgments

The study and the R/V *Tangaroa* voyages were funded by the consequences of ocean, Earth change program, and core funding to the National Institute of Water and Atmospheric Research. We would like to thank the captains from the TAN0803 and TAN1106 voyages Roger Goodison and Doug Monk, respectively, and the crew and scientists that participated in these voyages. We would also like to thank Thomas Max (NIWA) for running the stable isotopes, Kevin Mackay for providing GIS support, Mike Williams and Phil Sutton for their help and oceanographic expertise, and Sam Dean for his insights into the complexities of the SHWW. We would like to thank Tim Barrows and Karen Kohfeld for their constructive comments which have significantly improved the paper. This paper is a contribution to the INQUA supported Southern Hemisphere Assessment of Palaeo-Environments project. Data from this project is available from the Pangaea website http://doi.pangaea.de/10.1594/PANGAEA.846175.

References

Bals-Elsholz, T. M., E. H. Atallah, L. F. Bosart, T. A. Wasula, M. J. Cempa, and A. R. Lupo (2001), The wintertime Southern Hemisphere split jet: Structure, variability and evolution, *J. Clim.*, *14*, 4191–4215.

Barrows, T. T., and S. Juggins (2005), Sea-surface temperatures around the Australian margin and Indian Ocean during the Last Glacial Maximum, *Quat. Sci. Rev.*, *24*, 1017–1047.

Barrows, T. T., S. Juggins, P. De Deckker, J. Thiede, and J. I. Martinez (2000), Sea-surface temperatures of the southwest Pacific Ocean during the Last Glacial Maximum, *Paleoceanography*, *15*, 95–109, doi:10.1029/1999PA900047.

Barrows, T. T., S. Juggins, P. De Deckker, E. Calvo, and C. Pelejero (2007), Long term sea surface temperature and climate change in the Australian-New Zealand region, *Paleoceanography*, *22*, PA2215, doi:10.1029/2006PA001328.

Barrows, T. T., S. J. Lehman, L. K. Fifield, and P. De Deckker (2007a), Absence of cooling in New Zealand and the adjacent ocean during the Younger Dryas chronozone, *Science*, *318*, 86–89.

Barrows, T. T., S. Juggins, P. DeDeckker, E. Calvo, and C. Pelejero (2007b), Long term sea surface temperature and climate change in the Australian-New Zealand region, *Paleoceanography*, *22*, PA2215, doi:10.1029/2006PA001328.

Belkin, I. M., and A. L. Gordon (1996), Southern Ocean fronts from the Greenwich meridian to Tasmania, *J. Geophys. Res.*, *101*, 3675–3696, doi:10.1029/95JC02750.

Bi, J., and K. Bennett (2003), Regression error characteristic curves, in *Proceedings of the Twentieth International Conference on Machine Learning*, Washington, D. C., pp. 43–50, AAAI Press, Menlo Park, Calif.

Bianchi, C., and R. Gersonde (2004), Climate evolution at the last deglaciation: The role of the Southern Ocean, *Earth Planet. Sci. Lett.*, *228*, 407–424.

Bostock, H. C., B. N. Opdyke, M. K. Gagan, A. E. Kiss, and L. K. Fifield (2006), Glacial/interglacial changes in the East Australian current, *Clim. Dyn.*, *26*, 645–659, doi:10.1007/s00382-005-0103-7.

Bostock, H. C., et al. (2013), A review of the Australian-New Zealand sector of the Southern Ocean over the last 30 ka (Aus-INTIMATE project), *Quat. Sci. Rev.*, *74*, 35–57.

Boyd, P., J. LaRoche, M. Gall, R. Frew, and R. M. L. McKay (1999), Role of iron, light, and silicate in controlling algal biomass in subantarctic waters SE of New Zealand, *J. Geophys. Res.*, *104*, 13,391–13,404.

Breiman, L. (2001), Random Forests, *Mach. Learn.*, *45*, 5–32.

Burls, N. J., and C. J. C. Reason (2006), Sea surface temperature fronts in the midlatitude South Atlantic revealed by using microwave satellite data, *J. Geophys. Res.*, *111*, C08001, doi:10.1029/2005JC003133.

Butzin, M., M. Prange, and G. Lohmann (2005), Radiocarbon simulations for the glacial ocean: The effects of wind stress, Southern Ocean sea ice and Heinrich events, *Earth Planet. Sci. Lett.*, *235*, 45–61.

Calvo, E., C. Pelejero, G. A. Logan, and P. De Deckker (2004), Dust-induced changes in phytoplankton composition in the Tasman Sea during the last four glacial cycles, *Paleoceanography*, *19*, PA2020, doi:10.1029/2003PA000992.

Calvo, E., C. Pelejero, P. DeDeckker, and G. A. Logan (2007), Antarctic deglacial pattern in a 30 kyr record of sea surface temperature offshore South Australia, *Geophys. Res. Lett.*, *34*, L13707, doi:10.1029/2007GL029937.

Carter, L., and B. Manighetti (2006), Glacial/interglacial control of terrigenous and biogenic fluxes in the deep ocean off a high input, collisional margin: A 139 kyr-record from New Zealand, *Mar. Geol.*, *226*, 307–322.

Carter, L., and I. N. McCave (1997), The sedimentary regime beneath the deep western boundary current inflow to the southwest Pacific Ocean, *J. Sediment. Res.*, *67*, 1005–1017.

Carter, L., B. Manighetti, G. Ganssen, and L. Northcote (2008), Southwest pacific modulation of abrupt climate change during Antarctic Cold Reversal-Younger Dryas, *Palaeogeogr. Palaeoclimatol. Palaeoecol.*, *260*, 284–298.

Carter, R. M., P. R. Gammon, and L. Millwood (2004), Glacial-interglacial (MIS 1–10) migrations of the Subtropical Front across ODP Site 1119, Canterbury Bight, Southwest Pacific Ocean, *Mar. Geol.*, *205*, 29–58.

Chavaillaz, Y., F. Codron, and M. Kageyama (2013), Southern westerlies in LGM and future (RCP4.5) climates, *Clim. Past*, *9*, 517–524, doi:10.5194/cp-9-517-2013.

Chiswell, S. M. (1996), Variability in the Southland Current, New Zealand, *N. Z. J. Mar. Freshwater Res.*, *30*, 1–17.

Conway, C. E., H. C. Bostock, J. A. Baker, R. J. Wysoczanski, and A.-L. Verdier (2012), Evolution of Macquarie Ridge Complex seamounts: Implications for volcanic and tectonic processes at the Australia-Pacific plate boundary south of New Zealand, *Mar. Geol.*, *295–298*, 34–50.

Cortese, G., et al. (2013), Southwest Pacific Ocean response to a warmer world: Insights from marine isotope stage 5e, *Paleoceanography*, *28*, 1–14, doi:10.1002/palo.20052.

Crundwell, M., G. Scott, T. Naish, and L. Carter (2008), Glacial–interglacial ocean climate variability from planktonic foraminifera during the Mid-Pleistocene transition in the temperate Southwest Pacific, ODP Site 1123, *Palaeogeogr. Palaeoclimatol. Palaeoecol.*, *260*, 202–229.

Currie, K., M. Reid, and K. Hunter (2011), Interannual variability of carbon dioxide drawdown by subantarctic surface water near New Zealand, *Biogeochemistry*, *104*, 23–34.

De Boer, A. M., R. M. Graham, M. D. Thomas, and K. E. Kohfeld (2013), The control of the Southern Hemisphere westerlies on the position of the Subtropical Front, *J. Geophys. Res. Oceans*, *118*, 1–7, doi:10.1002/jgrc.20407.

De Deckker, P., M. Moros, K. Perner, and E. Jansen (2012), Influence of the tropics and southern westerlies on glacial interhemispheric asymmetry, *Nat. Geosci.*, *5*, 266–269, doi:10.1038/NGEO1431.

Deacon, G. (1982), Physical and biological zonation in the southern Ocean, *Deep Sea Res., Part A*, *29*, 1–15.

Fenner, J., and A. di Stefano (2004), Late Quaternary oceanic fronts along Chatham Rise indicated by phytoplankton assemblages, and refined calcareous nannofossil stratigraphy for the mid-latitude SW Pacific, *Mar. Geol.*, *205*, 59–86.

Fernandez, D., M. Bowen, and L. Carter (2014), Intensification and variability of the confluence of subtropical and subantarctic boundary currents east of New Zealand, *J. Geophys. Res. Oceans*, *119*, 1146–1160, doi:10.1002/2013JC009153.
Govin, A., E. Michel, L. Labeyrie, C. Waelbroeck, F. Dewilde, and E. Jansen (2009), Evidence for northward expansion of Antarctic Bottom Water mass in the Southern Ocean during the last glacial inception, *Paleoceanography*, *24*, PA1202, doi:10.1029/2008PA001603.
Graham, R. M., and A. M. De Boer (2013), The dynamical Subtropical Front, *J. Geophys. Res. Oceans*, *118*, 1–10, doi:10.1002/jgrc.20408.
Hamilton, L. J. (2006), Structure of the subtropical front in the Tasman Sea, *Deep Sea Res., Part I*, *53*, 1989–2009.
Hayward, B. W., A. Sabaa, and H. R. Grenfell (2004), Benthic foraminifera and the late Quaternary (last 150 ka) paleoceanographic and sedimentary history of the Bounty Trough, east of New Zealand, *Palaeogeogr. Palaeoclimatol. Palaeoecol.*, *211*, 59–93.
Hayward, B. W., et al. (2008), The effect of submerged plateaux on Pleistocene gyral circulation and sea-surface temperatures in the Southwest Pacific, *Global Planet. Change*, *63*, 309–316.
Hayward, B. W., A. T. Sabaa, A. Kolodziej, M. P. Crundwell, S. Steph, G. H. Scott, H. L. Neil, H. C. Bostock, L. Carter, and H. R. Grenfell (2012), Planktic foraminifera-based sea-surface temperature record in the Tasman Sea and history of the Subtropical Front around New Zealand over the last one million years, *Mar. Micropaleontol.*, *82–83*, 13–27.
Hayward, B. W., A. T. Sabaa, H. R. Grenfell, H. Neil, and H. Bostock (2013), Ecological distribution of recent deep-water foraminifera around New Zealand, *J. Foraminiferal. Res.*, *43*, 415–442.
Heath, R. A. (1985), A review of physical oceanography of the seas around New Zealand – 1982, *N. Z. J. Mar. Freshwater Res.*, *19*, 79–124.
Higham, T. F. G., and A. G. Hogg (1995), Radiocarbon dating of prehistoric shell from New Zealand and calculation of the ΔR value using fish otoliths, *Radiocarbon*, *37*, 409–416.
Hill, K. L., S. R. Rintoul, R. Coleman, and K. R. Ridgway (2008), Wind forced low frequency variability of the east Australian current, *Geophys. Res. Lett.*, *35*, L08602, doi:10.1029/2007GL032912.
Hopkins, J., A. G. P. Shaw, and P. Challenor (2010), The Southland Front, New Zealand: Variability and ENSO correlations, *Cont. Shelf Res.*, *30*, 1535–1548.
Howard, W. R., and W. L. Prell (1992), Late Quaternary surface circulation of the Southern Indian Ocean and its relationship to orbital variations, *Paleoceanography*, *7*, 79–117, doi:10.1029/91PA02994.
Hutson, W. H. (1980), The Agulhas current during the late Pleistocene: Analysis of modern faunal analogs, *Science*, *207*, 64–66.
Jones, G. A., and P. Kaiteris (1983), A vacuum gasometric technique for rapid and precise analysis of calcium carbonate in sediments and soils, *J. Sediment. Petrol.*, *53*, 655–660.
Kidston, J., A. S. Taschetto, D. W. J. Thompson, and M. H. England (2011), The influence of Southern Hemisphere sea-ice extent on the latitude of the mid-latitude jet stream, *Geophys. Res. Lett.*, *38*, L15804, doi:10.1029/2011GL048056.
King, A. L., and W. R. Howard (2001), Seasonality of foraminiferal flux in sediment traps at Chatham Rise, SW Pacific: Implications for paleotemperature estimates, *Deep Sea Res., Part I*, *48*, 1687–1708.
Kohfeld, K. E., R. M. Graham, A. M. de Boer, L. C. Sime, E. W. Wolff, C. Le Quere, and L. Bopp (2013), Southern Hemisphere westerly wind changes during the Last Glacial Maximum: paleo-data synthesis, *Quat. Sci. Rev.*, *68*, 76–95.
Kostianoy, A. G., A. I. Ginzburg, M. Frankignoulle, and B. Delille (2004), Fronts in the southern Indian Ocean as inferred from satellite sea surface temperature data, *J. Mar. Syst.*, *45*, 55–73.
Lamy, L., R. Kilian, H. W. Arz, J.-P. Francois, J. Kaiser, M. Prange, and T. Steinke (2010), Holocene changes in the position and intensity of the southern westerly wind belt, *Nat. Geosci.*, *3*, 695–699, doi:10.1038/NGEO959.
Lauderdale, J. M., A. C. Naveira Garabato, K. I. C. Oliver, M. J. Follows, and R. G. Williams (2013), Wind-driven changes in Southern Ocean residual circulation, *Clim. Dyn.*, *41*, 2145–2164, doi:10.1007/s00382-012-1650-3.
Le, J., and N. J. Shackleton (1992), Carbonate dissolution fluctuations in the western equatorial Pacific during the late Quaternary, *Paleoceanography*, *7*, 21–42, doi:10.1029/91PA02854.
Lisiecki, L. E., and M. E. Raymo (2005), A Pliocene-Pleistocene stack of 57 globally distributed benthic $\delta^{18}O$ records, *Paleoceanography*, *20*, PA1003, doi:10.1029/2004PA001071.
Lüer, V., C. J. Hollis, and H. Willems (2008a), Late Quaternary radiolarian assemblages as indicators of paleoceanographic changes north of the subtropical front, offshore eastern New Zealand, southwest Pacific, *Micropaleontology*, *54*, 49–69.
Lüer, V., G. Cortese, H. L. Neil, C. J. Hollis, and H. Willems (2008b), Radiolarian-based sea surface temperatures and paleoceanographic changes during the Late Pleistocene–Holocene in the subantarctic southwest Pacific, *Mar. Micropaleontol.*, *70*, 151–165.
Marr, J. P., L. Carter, H. C. Bostock, A. Bolton, and E. Smith (2013), Southwest Pacific Ocean response to a warming world: Using Mg/Ca, Zn/Ca, and Mn/Ca in foraminifera to track surface ocean water masses during the last deglaciation, *Paleoceanography*, *28*, 1–16, doi:10.1002/palo.20032.
Martinez, J. I. (1994), Late Pleistocene paleoceanography of the Tasman Sea – implications for the dynamics of the warm pool in the Western Pacific, *Palaeogeogr. Palaeoclimatol. Palaeoecol.*, *112*, 19–62.
Molfino, B., N. G. Kipp, and J. J. Morley (1982), Comparison of foraminiferal, coccolithophorid and radiolarian paleotemperature equations: assemblage coherency and estimate concordancy, *Quat. Res.*, *17*, 279–313.
Morigi, C., L. Capotondi, F. Giglio, L. Langone, M. Brilli, B. Turi, and M. Ravaioli (2003), A possible record of the Younger Dryas event in deep-sea sediments of the Southern Ocean (Pacific sector), *Palaeogeogr. Palaeoclimatol. Palaeoecol.*, *198*, 265–278.
Moros, M., P. De Deckker, E. Jansen, K. Perner, and R. J. Telford (2009), Holocene climate variability in the Southern Ocean recorded in a deep-sea sediment core off South Australia, *Quat. Sci. Rev.*, *28*, 1932–1940.
Morris, M., B. Stanton, and H. Neil (2001), Subantarctic oceanography around New Zealand: Preliminary results from an ongoing survey, *N. Z. J. Mar. Freshwater Res.*, *35*, 499–519.
Neil, H. L., L. Carter, and M. Y. Morris (2004), Thermal isolation of Campbell Plateau, New Zealand, by the Antarctic Circumpolar Current over the past 130 kyr, *Paleoceanography*, *19*, PA4008, doi:10.1029/2003PA000975.
Nelson, C. S., P. J. Cooke, C. H. Hendy, and A. M. Cuthbertson (1993), Oceanographic and climatic changes over the past 160,0000 years at the Deep Sea Drilling Project Site 594 off southeastern New Zealand, Southwest Pacific Ocean, *Paleoceanography*, *8*, 435–458.
Nelson, C. S., I. L. Hendy, H. L. Neil, C. H. Hendy, and P. P. E. Weaver (2000), Last glacial jetting through the subtropical convergence zone in the Southwest Pacific off eastern New Zealand and some geological implications, *Palaeogeogr. Palaeoclimatol. Palaeoecol.*, *156*, 103–121.
Northcote, L. C., and H. L. Neil (2005), Seasonal variations in the foraminiferal flux in the Southern Ocean, Campbell Plateau, New Zealand, *Mar. Micropaleontol.*, *56*, 122–137.
Orsi, A. H., T. Whitworth III, and W. D. Nowlin Jr. (1995), On the meridional extent and fronts of the Antarctic Circumpolar Current, *Deep Sea Res., Part I*, *42*, 641–673, doi:10.1016/0967-0637(95)00021-W.
Pahnke, K., and J. P. Sachs (2006), Sea surface temperatures of southern mid-latitudes 0–160 kyr B.P., *Paleoceanography*, *21*, PA2003, doi:10.1029/2005PA001191.

Pahnke, K., and R. Zahn (2005), Southern Hemisphere water mass conversion linked to North Atlantic climate variability, *Science*, *307*, 1741–1746.
Pahnke, K., R. Zahn, H. Elderfield, and M. Schulz (2003), 340,000 year centennial scale marine record of Southern Hemisphere climatic oscillation, *Science*, *301*, 948–952.
Passlow, V., W. Pinxian, and A. R. Chivas (1997), Late Quaternary palaeoceanography near Tasmania, Southern Australia, *Palaeogeogr. Palaeoclimatol. Palaeoecol.*, *131*, 433–463.
Pedro, J. B., T. D. van Ommen, S. O. Rasmussen, V. I. Morgan, J. Chappellaz, A. D. Moy, V. Masson-Delmotte, and M. Delmotte (2011), The last deglaciation: Timing the bipolar see-saw, *Clim. Past*, *7*, 671–683.
Pelejero, C., E. Calvo, T. T. Barrows, G. A. Logan, and P. De Deckker (2006), South Tasman Sea alkenone palaothermometry over the last four glacial/interglacial cycles, *Mar. Geol.*, *230*, 73–86.
Pena-Ortiz, C., D. Gallego, P. Ribera, P. Ordonez, and M. D. C. Alvarez-Castro (2013), Observed trends in the global jet stream characteristics during the second half of the 20th century, *J. Geophys. Res. Atmos.*, *118*, 2702–2713, doi:10.1002/jgrd.50305.
Rafter, T. A., H. S. Jansen, L. Lockerbie, and M. M. Trotter (1972), New Zealand reference standards, in *International Conference on ^{14}C Dating, Proceedings 8th Wellington*, vol. 2, edited by T. A. Rafter and T. Grant-Taylor, pp. H29–H79, R. Soc. of New Zealand, Wellington.
Reeves, J. M., et al. (2013), Palaeoenvironmental change in tropical Australasia over the last 30,000 years - A synthesis by the OZ-INTIMATE group, *Quat. Sci. Rev.*, *74*, 97–114.
Roche, D. M., H. Renssen, D. Paillard, and G. Lavavasseur (2011), Deciphering the spatio-temporal complexity of climate change of the last deglaciation: A model analysis, *Clim. Past*, *7*, 591–602, doi:10.5194/cp-7-591-2011.
Rojas, M., P. Moreno, M. Kageyama, M. Crucifix, C. Hewitt, A. Abe, R. Ohgaito, E. Brady, and P. Hope (2009), The last glacial maximum in the Southern Hemisphere in PMIP2 simulations, *Clim. Dyn.*, *32*, 525–547.
Sallée, J. B., K. Speer, and R. Morrow (2008), Response of the Antarctic Circumpolar Current to atmospheric variability, *J. Clim.*, *21*, 3020–3039, doi:10.1175/2007JCLI1702.1.
Schaefer, G., J. S. Rodger, B. W. Hayward, J. P. Kennett, A. T. Sabaa, and G. H. Scott (2005), Planktic foraminiferal and sea surface temperature record during the last 1 Myr across the Subtropical Front, Southwest Pacific, *Mar. Micropaleontol.*, *54*, 191–212.
Schlitzer, R., (2009), Ocean Data View Software. [Available at http://odv.awi.de/.]
Schuur, C., M. F. Coffin, C. Frohlich, C. Massell, G. Kamer, D. Ramsay, and D. W. Caress (1998), Sedimentary regimes at the Macquarie Ridge Complex: Interaction of Southern Ocean circulation and plate boundary bathymetry, *Paleoceanography*, *13*, 646–670, doi:10.1029/98PA02357.
Scott, G. H. (2013), Planktonic foraminifera as oceanographic proxies: Comparison of biogeographic classifications using some southwest Pacific core-top faunas, *Adv. Oceanogr.*, 508184, doi:10.5402/2013/508184.
Shaw, A., and R. Vennell (2001), Measurements of an oceanic front using a front-following algorithm for AVHRR SST imagery, *Remote Sens. Environ.*, *75*, 47–62.
Shevenell, A. E., A. E. Ingalls, E. W. Domack, and C. Kelly (2011), Holocene Southern Ocean surface temperature variability west of the Antarctic Peninsula, *Nature*, *470*, 250–254, doi:10.1038/nature09751.
Shulmeister, J., et al. (2004), The Southern Hemisphere westerlies in the Australasian sector over the last glacial cycle: A synthesis, *Quat. Int.*, *118–119*, 23–53.
Sikes, E. L., and J. K. Volkman (1993), Calibration of alkenone unsaturation ratios ($U^{K'}_{37}$) for paleotemperature estimation, *Geochim. Cosmochim. Acta*, *57*, 1883–1889.
Sikes, E. L., J. K. Volkmann, L. G. Robertson, and J.-J. Pichon (1997), Alkenones and alkenes in surface waters and sediments of the Southern Ocean: Implications for paleotemperature estimation in polar regions, *Geochim. Cosmochim. Acta*, *61*, 1495–1505.
Sikes, E. L., C. Samson, T. Guilderson, and W. R. Howard (2000), Old radiocarbon ages in the southwest Pacific Ocean during the last glacial period and deglaciation, *Nature*, *405*, 555–559.
Sikes, E. L., W. R. Howard, H. L. Neil, and J. K. Volkman (2002), Glacial-interglacial sea surface temperature changes across the subtropical front east of New Zealand based on alkenone unsaturation ratios and foraminiferal assemblages, *Paleoceanography*, *17*(2), 1012, doi:10.1029/2001PA000640.
Sikes, E. L., S. D. Nodder, T. O'Leary, and J. K. Volkman (2005), Alkenone temperature records and biomarker flux at the Subtropical Front on the Chatham Rise, SW Pacific Ocean, *Deep Sea Res., Part I*, *52*, 721–748.
Sikes, E. L., W. R. Howard, C. R. Samson, T. S. Mahan, L. G. Robertson, and J. K. Volkman (2009), Southern Ocean seasonal temperature and Subtropical Front movement on the South Tasman Rise in the late Quaternary, *Paleoceanography*, *24*, PA2201, doi:10.1029/2008PA001659.
Sime, L. C., K. E. Kohfeld, C. Le Quéré, E. W. Wolff, A. M. de Boer, R. M. Graham, and L. Bopp (2013), Southern Hemisphere westerly wind changes during the Last Glacial Maximum: Model-data comparison, *Quat. Sci. Rev.*, *64*, 104–120.
Smith, R. O., R. Vennell, H. C. Bostock, and M. J. M. Williams (2013), Interaction of the subtropical front with topography around southern New Zealand, *Deep Sea Res., 1*, *76*, 13–26.
Sokolov, S., and S. R. Rintoul (2002), Structure of Southern Ocean fronts at 140°E, *J. Mar. Syst.*, *37*, 151–184.
Sokolov, S., and S. R. Rintoul (2009), Circulation structure and distribution of the Antarctic Circumpolar Current fronts: 1. Mean circumpolar paths, *J. Geophys. Res.*, *114*, C11018, doi:10.1029/2008JC005108.
Sokolov, S., S. R. Rintoul, and B. Wienecke (2006), Tracking the Polar Front south of New Zealand using penguin dive data, *Deep Sea Res., Part I*, *53*, 591–607.
Stuiver, M., and P. J. Reimer (1993), Extended ^{14}C data base and revised CALIB 3.0 ^{14}C age calibration program, *Radiocarbon*, *35*, 215–230.
Sutton, P. J. H. (2001), Detailed structure of the subtropical front over Chatham Rise, east of New Zealand, *J. Geophys. Res.*, *106*, 31,045–31,056, doi:10.1029/2000JC000562.
Sutton, P. J. H. (2003), The Southland Current: A subantarctic current, *N. Z. J. Mar. Freshwater Res.*, *37*, 645–652.
Taljaard, J. J. (1972), Synoptic meteorology of the Southern Hemisphere, in *Meteorology of the Southern Hemisphere*, edited by D. J. Karoly and D. G. Vincent, pp. 139–211, Am. Meteorol. Soc.
Thompson, D. W. J., and J. M. Wallace (2000), Annular modes in the extratropical circulation. Part I: Month-to-month variability, *J. Clim.*, *13*, 1000–1016.
Tilburg, C. E., H. E. Hurlburt, J. J. O'Brien, and J. F. Shriver (2001), The dynamics of the East Australian Current System: The Tasman Front, the East Auckland Current, and the East Cape Current, *J. Phys. Oceanogr.*, *31*, 2917–2943.
Ummenhofer, C. C., P. C. McIntosh, M. J. Pook, and J. S. Risbey (2013), Impact of surface forcing on Southern Hemisphere atmospheric blocking in the Australia-New Zealand sector, *J. Clim.*, *26*, 8476–8494, doi:10.1175/JCLI-D-12-00860.1.

Vázquez Riveiros, N., C. Waelbroeck, L. Skinner, D. M. Roche, J.-C. Duplessy, and E. Michel (2010), Response of South Atlantic deep waters to deglacial warming during Terminations V and I, *Earth Planet. Sci. Lett.*, *298*, 323–333.

Voigt, I., C. M. Chiessi, M. Prange, S. Mulitza, J. Groeneveld, V. Varma, and R. Henrich (2015), Holocene shifts of the southern westerlies across the South Atlantic, *Paleoceanography*, *30*, 39–51, doi:10.1002/2014PA002677.

Volkmann, J. K., S. M. Barrett, S. I. Blackburn, and E. L. Sikes (1995), Alkenones in Gephyrocapsa oceanica: Implications for paleoclimatic studies, *Geochim. Cosmochim. Acta*, *59*, 513–520.

Weaver, P. P. E., H. L. Neil, and L. Carter (1997), Sea surface temperature estimates from the Southwest Pacific based on planktonic foraminifera and oxygen isotopes, *Palaeogeogr. Palaeoclimatol. Palaeoecol.*, *131*, 241–256.

Weaver, P. P. E., L. Carter, and H. L. Neil (1998), Response of surface water masses and circulation to late Quaternary climate change east of New Zealand, *Paleoceanography*, *13*, 70–83, doi:10.1029/97PA02982.

Wilson, K., B. W. Hayward, A. Sabaa, G. H. Scott, and J. P. Kennett (2005), A one-million year history of a north–south segment of the Subtropical Front, east of New Zealand, *Paleoceanography*, *20*, PA2004, doi:10.1029/2004PA001080.